Redox Biology 41 (2021) 101932

Contents lists available at ScienceDirect

Redox Biology

journal homepage: www.elsevier.com/locate/redox

Exosomal miR-155 from M1-polarized macrophages promotes EndoMT and impairs mitochondrial function via activating NF-κB signaling pathway in vascular endothelial cells after traumatic spinal cord injury

Xuhui Ge [a,1], Pengyu Tang [a,1], Yuluo Rong [a,1], Dongdong Jiang [a], Xiao Lu [b], Chengyue Ji [a], Jiaxing Wang [a], Chenyu Huang [c], Ao Duan [a], Yang Liu [d], Xinglin Chen [e], Xichen Chen [f], Zhiyang Xu [f], Feng Wang [f], Zibin Wang [f], Xiaoyan Li [f], Wene Zhao [f], Jin Fan [a], Wei Liu [a,**], Guoyong Yin [a,***], Weihua Cai [a,*]

[a] Department of Orthopedics, The First Affiliated Hospital of Nanjing Medical University, Nanjing, 210029, Jiangsu, China
[b] Department of Orthopedics, Dongtai Hospital Affiliated to Nantong University, Yancheng, 224200, Jiangsu, China
[c] Department of Orthopedics, Nanjing First Hospital, Nanjing Medical University, Nanjing, 210006, Jiangsu, China
[d] Department of Orthopedics, The Affiliated Wuxi No.2 People's Hospital of Nanjing Medical University, Wuxi, 214002, Jiangsu, China
[e] Department of Urology, The First Affiliated Hospital of Nanjing Medical University, Nanjing, 210029, Jiangsu, China
[f] Department of Analytical & Testing Center, Nanjing Medical University, Nanjing, 211166, Jiangsu, China

ARTICLE INFO

Keywords:
Spinal cord injury
Blood-spinal-cord-barrier
miR-155/SOCS6/p65
Endothelial-to-mesenchymal transition
Mitochondria

ABSTRACT

Pathologically, blood-spinal-cord-barrier (BSCB) disruption after spinal cord injury (SCI) leads to infiltration of numerous peripheral macrophages into injured areas and accumulation around newborn vessels. Among the leaked macrophages, M1-polarized macrophages are dominant and play a crucial role throughout the whole SCI process. The aim of our study was to investigate the effects of M1-polarized bone marrow-derived macrophages (M1-BMDMs) on vascular endothelial cells and their underlying mechanism. Microvascular endothelial cell line bEnd.3 cells were treated with conditioned medium or exosomes derived from M1-BMDMs, followed by evaluations of endothelial-to-mesenchymal transition (EndoMT) and mitochondrial function. After administration, we found conditioned medium or exosomes from M1-BMDMs significantly promoted EndoMT of vascular endothelial cells *in vitro* and *in vivo*, which aggravated BSCB disruption after SCI. In addition, significant dysfunction of mitochondria and accumulation of reactive oxygen species (ROS) were also detected. Furthermore, bioinformatics analysis demonstrated that miR-155 is upregulated in both M1-polarized macrophages and microglia. Experimentally, exosomal transfer of miR-155 participated in M1-BMDMs-induced EndoMT and mitochondrial ROS generation in bEnd.3 cells, and subsequently activated the NF-κB signaling pathway by targeting downstream suppressor of cytokine signaling 6 (SOCS6), and suppressing SOCS6-mediated p65 ubiquitination and degradation. Finally, a series of rescue assay further verified that exosomal miR155/SOCS6/p65 axis regulated the EndoMT process and mitochondrial function in vascular endothelial cells. In summary, our work revealed a potential mechanism describing the communications between macrophages and vascular endothelial cells after SCI which could benefit for future research and aid in the development of potential therapies for SCI.

1. Background

Spinal cord injury (SCI) is a devastating central nervous system (CNS) consequence with motor, sensory, and autonomic dysfunction. Pathophysiologically, the blood-brain barrier (BBB) or blood-spinal-cord barrier (BSCB) is ruptured after SCI, usually occurring within 5

* Corresponding author.
** Corresponding author.
*** Corresponding author.
E-mail addresses: liuweiorth@njmu.edu.cn (W. Liu), guoyong_yin@sina.com (G. Yin), caiwhspine@sina.com (W. Cai).
[1] These authors contributed equally.

https://doi.org/10.1016/j.redox.2021.101932
Received 9 December 2020; Received in revised form 1 March 2021; Accepted 1 March 2021
Available online 5 March 2021

min and lasting up to 28 days after SCI [1,2], leading to edema, inflammatory response, progressive neuron death, and glial cells activation [3]. Physiologically composed of continuous endothelial cells, pericytes, and glial cells with molecular junctions, the BSCB limits paracellular and transcellular transport in the CNS, while its dysfunction after SCI results in the infiltration of peripheral inflammatory cells and factors into the lesion and causes secondary SCI [4]. In contrast to highly permeable peripheral capillary endothelium, the BSCB endothelium is sealed mainly by tight junctions (TJs). Previous studies have reported the breakdown of TJs in brain injury and SCI [5–7], and preventing disruption of TJs might alleviate edema secondary to BSCB dysfunction [8]. It should be mentioned that endothelial-to-mesenchymal transition (EndoMT) plays a key role in TJs loss. EndoMT is a dynamic cell transformation from the endothelial state towards the mesenchymal state along with loss of endothelial characteristics like TJs and acquisition of mesenchymal, fibroblast, or stem-cell-like features [9]. Notably, EndoMT cells are predominately located nearby blood vessels [10]. Many previous studies have focused on the role of EndoMT in cancer development, however, the relationship between BSCB disruption and EndoMT is unclear.

Both the CNS cells in the neurovascular unit and blood-borne peripheral cells constantly modulate the BSCB and influence its breakdown and repair after SCI [11], however, a significant amount of research in the past few years has focused on the effects of astrocytes and pericytes on BSCB homeostasis, yet the role of macrophages/microglia in the BSCB has been seldom defined. Current data indicate that a large number of peripheral macrophages will enter the injured spinal cord and trigger a cascade of responses after SCI [12]. It was showed that macrophages have two polarization states including "classically-activated", proinflammatory, cytotoxic M1 phenotype and "alternatively-activated", anti-inflammatory, pro-repair M2 phenotype [13]. Although both M1 and M2 macrophages are present at the injured site, M1 polarization plays a dominant role throughout the whole SCI process. Especially in the early stages, the SCI lesion is comprised predominately of M1 macrophages [14], inducing BSCB disruption via neuroinflammation and endothelial cells apoptosis; in the delayed phase, these M1 macrophages will be partly transformed to anti-inflammatory phenotype, repairing BSCB breakdown [15]. Presently, the underlying mechanism of macrophages-induced BSCB dysfunction is still unclear and needs further investigation.

Exosomes are a type of extracellular vesicle containing different constituents including proteins, metabolites, liquids and nucleic acids [16,17]. Over the past few years, exosomes have been investigated in SCI as a treatment strategy or as a cell crosstalk medium [18,19]. Recent evidence demonstrated that macrophages-derived exosomes promote axonal degeneration by delivering functional NADPH oxidase 2 complexes to injured axons [20]. Moreover, small extracellular vesicles derived from M2 bone marrow could attenuate apoptosis and promote motor function recovery following SCI [21]. However, it remains unclear whether M1 macrophages-derived exosomes regulate BSCB integrity, and the underlying mechanisms still need further investigation.

'Reactive oxygen species' (ROS) is a general term for a group of oxygen molecules derived from reduction–oxidation reactions or by electronic excitation. It has an inseparable relationship with mitochondria, and accumulated ROS has been implicated in the loss of mitochondrial homeostasis and energy impairment [22]. After SCI, mitochondrial ROS increase has been detected within 24 h [23], and inhibition of ROS production might protect injured spinal cord from mitochondrial oxidative stress and neuronal apoptosis [24]. There is evidence that ROS level of vascular endothelial cells is upregulated in cerebrovascular disease, and it subsequently impairs the integrity of BBB [25]. Therefore, it is necessary to maintain mitochondrial homeostasis in vascular endothelial cells after SCI.

In this present study, we demonstrated that infiltrated macrophages after SCI could aggravate BSCB integrity breakdown by promoting EndoMT and impairing mitochondrial function in vascular endothelial cells via delivering exosomal miR-155, which subsequently activates the NF-κB pathway by suppressing SOCS6-induced p65 degradation. Our study proposed an unreported theory which may help to better understand the underlying mechanism of SCI and provide a promising target for treating SCI.

2. Material and methods

2.1. Microarray data

The GSE33453, GSE49329 and GSE49330 datasets comparing PBS- and LPS-treated macrophages or microglia were downloaded from the Gene Expression Omnibus (GEO, https://www.ncbi.nlm.nih.gov/geo/) database. Following normalization, $\log_2$ transform, and probe annotation, genes with $|\log2 \text{ fold change}| > 1.5$ and adjusted P value < 0.05 were identified as differentially expressed genes (DEGs). The hub DEGs were then identified for further investigation.

2.2. Cell culture

The primary bone marrow-derived macrophages (BMDMs) were obtained and cultured as previously reported [21]. The femur and tibia of 4-week-old mice were removed, from which bone marrow was flushed out with cold PBS. Following filtration through a 70-μm strainer, a 5 mL red blood cells lysis buffer was added to remove red blood cells. After centrifugation, cells were washed twice and resuspended in Dulbecco's modified Eagle's medium (DMEM) containing 10% FBS, 1% penicillin-streptomycin, and 20 ng/mL M-CSF (R&D System, USA). To induce M1 polarization, BMDMs were treated with LPS (1 μg/mL) for 24 h and flow cytometry was used to identify polarization. In addition, BMDMs-derived exosomes were extracted from supernatant for further study.

The bEnd.3 brain microvascular endothelial cell line was purchased from the Type Culture Collection of the Chinese Academy of Sciences (Shanghai, China). Cells were cultured in the DMEM containing 10% FBS and 1% penicillin-streptomycin at 37 °C and 5% CO_2.

2.3. Exosomes isolation and identification

Exosomes were extracted from the culture supernatant of BMDMs pretreated with and without LPS. Prior to culture medium collection, BMDMs were washed twice with PBS and the medium was replaced by exosome-free medium upon LPS stimulation. Conditioned medium was collected after 24 h and was centrifuged at 300 g for 10 min and 2000 g for 10 min. After centrifugation, cell supernatant was filtered through a 0.22 μm filter to remove cellular debris. The supernatant was subsequently transferred to an Amicon Ultra-15 centrifugal filter (Millipore, USA) and centrifuged at 4000 g until the volume in upper chamber was reduced to approximately 200 μL. For exosomes purification, the liquid in upper chamber was loaded on the 30% sucrose/D2O cushion and subjected to ultracentrifugation at 100,000 g (Beckman Coulter) for 60 min at 4 °C. The pallet was then suspended in PBS for further identification and administration.

The transmission electron microscope (TEM, Tecnai 12; Philips, Best, The Netherlands) was used to characterize the morphology of exosomes. Nanoparticle tracking analysis (NTA, Nanosight Ltd., Navato, CA) was used to measure the diameter and particle number of exosomes. Western blot analysis was performed to examine surface biomarkers of exosomes.

2.4. Uptake of exosomes by bEnd.3 cells

Dil solution (4 mg/mL, Molecular probe, USA) was incubated with exosomes-containing PBS solution for fluorescent labeling. Excessive dye was removed through centrifugation at 100,000 g at 4 °C, and labeled exosomes were washed three times. These Dil-labeled-exosomes

were co-cultured with bEnd.3 cells for 24 h, and the cells were then washed with PBS and fixed in 4% paraformaldehyde. Uptake of exosomes by bEnd.3 cells was optically examined using laser confocal microscopy (Carl Zeiss Microscopy GmbH, Germany).

2.5. Transepithelial electrical resistance (TEER) measurement

The bEnd.3 cells were seeded in an insert with 0.4 μm pore (Millipore, USA) and allowed to reach a confluent state. Before every measurement, cells were preequilibrated with HBSS for 30 min and resistance was measured using a Millicell® ERS instrument (Millipore, USA) according to the manufacturer's instructions. TEER values were calculated using the formula: TEER (Ω•cm [2]) = [TEER total - TEER blank] × membrane area.

2.6. Permeability assay

Transepithelial permeability was measured using FITC-dextran (4 kDa, Sigma Aldrich, USA). Cells were seeded in the above-mentioned insert and allowed to reach confluence, 100 μl of FITC-dextran medium (1 mg/mL) was added to the apical chamber and 500 μl of medium was added to the basal chamber. After incubation for 2 h, culture medium in the basal chamber was collected for fluorescence measurement using a fluorescence spectrophotometer (ThermoFisher Scientific, USA).

2.7. Measurement of oxygen consumption rate (OCR)

The Seahorse FX24 Extracellular Flux Analyzer (Seahorse Biosciences, North Billerica, MA, USA) was employed as previously described [26]. OCR was tested by sequentially adding 2 μM oligomycin (an ATP synthase blocker), 1 μM carbonyl cyanide 4-(trifluoromethoxy) phenylhydrazone (FCCP, the mitochondrial uncoupler), 1 μM antimycin A and 1 μM rotenone (A&R, inhibitors of complex I and III). The XFe Wave software (Seahorse Biosciences) was used to quantify results. The basal respiration, ATP production, respiratory capacity (maximal electron transport chain activity) and respiratory reserve (flexibility with increased energy demand) were calculated according to the manufacturer's protocol.

2.8. Mitochondrial membrane potential measurement, mitochondrial ROS detection, and ROS evaluation

The mitochondrial membrane potential was evaluated using the JC-1 Assay Kit (Beyotime, China) followed by flow cytometry analysis according to the manufacturer's protocol. The mitochondrial potential was quantified using aggregate-to-monomer (red/green) fluorescence intensity ratio. The mitochondrial ROS was detected using a MitoSOX™ Red Mitochondrial Superoxide Indicator (Molecular Probes, USA) according to the manufacturer's protocol, and observed under a confocal microscope. The ROS levels were evaluated via 2',7'-dichlorofluorsecein-diacetate (DCFH-DA) by the ROS Assay Kit (Beyotime, China) followed by flow cytometry analysis according to the manufacturer's protocol.

2.9. Morphological analysis of mitochondria

The bEnd.3 cells were incubated with 100 nM Mitotracker Red CMXRos (Invitrogen) for 30 min at 37 °C according to the manufacturer's protocol. The fluorescent images were acquired using a confocal microscope. The mitochondrial morphology was quantified using Image J (with Fiji MiNA plugin), as previously described [27].

2.10. Immunofluorescence assay

Cells or tissue sections were fixed with 4% polyoxymethylene and permeabilized with 0.3% Triton X-100, then blocked with 5% BSA, and finally incubated with corresponding primary antibodies at 4 °C overnight. Corresponding secondary antibodies and DAPI reagent were used to treat cells and sections the following day, and immunoactivity was visualized under a fluorescence microscope.

2.11. RNA extraction and qRT-PCR

Total RNA of cells and exosomes was extracted with TRIzol reagent (Takara, Japan). The cDNA of miRNA and mRNA were synthesized by Hairpin-itTM miRNA qPCR Quantitation Kit (GenePharma, China) and PrimeScript RT reagent Kit (Takara, Japan), respectively. The qRT-PCR assay was subsequently performed with the TB Green® Premix Ex TaqTM kit (Takara, Japan). Expression levels of mRNA and miRNA were respectively normalized to GAPDH and U6, respectively. The relative expression was calculated using the $2^{-\Delta\Delta CT}$ method.

2.12. Western blot assay

Proteins of cells or tissues were extracted by RIPA lysis (Beyotime, China). Protein concentration was examined by BCA (Beyotime, China). Following denaturation and separation in the SDS-PAGE gels, proteins were transferred to PVDF membranes; the membranes were then blocked by blocking buffer (Beyotime, China) for 1 h at room temperature and incubated with primary antibodies at 4 °C overnight. After washing with TBST and incubation with corresponding secondary antibodies for 2 h, the protein bands were visualized by a PowerOpti-ECL detection system (ThermoFisher Scientific, USA).

2.13. Co-immunoprecipitation (Co-IP) assay

The Co-IP assay was conducted using Co-IP kit (Piercm™, ThermoFisher Scientific) following the manufacturer's protocol. Cell lysates of bEnd.3 cells were prepared in lysis buffer and then incubated with agarose beads-conjugated antibodies at 4 °C overnight with gentle rotation. Following washing with lysis buffer, proteins bound to beads were eluted by elution buffer for subsequent immunoblot.

2.14. Preparation of contusive spinal cord injury mouse model and experimental groups

All the animal experiments were carried out with the approval of the Committee on the Ethics of Animal Experiments of Nanjing Medical University. The contusion model of SCI in our work was carried out as previously described [28,29]. Mice were anesthetized by isofluorane inhalation and underwent a laminectomy at vertebral level T8. The vertebral column was stabilized and exposed dorsal surface of the cord was subjected to a weight drop injury using a 5-g rod dropped from a height of 6.5 cm using the spinal cord impactor (68097, RWD, USA). After the impact, successful SCI was verified by body trembling, swaying of the tail, and a fluttering retraction of the hind limbs and body. The bladder function following SCI is impaired, so auxiliary urination was performed twice daily until bladder function was restored.

Mice after SCI were randomly divided into two groups, an SCI-only group and an M1-Exos treatment group. The two groups were administered PBS (200 μL) and M1-Exos (200 μg of total exosomal protein in 200 μL of PBS) just for once, respectively, by tail injection immediately following SCI as we previously described [28,30].

2.15. Behavioral assessment

2.15.1. Basso mouse scale (BMS) behavioral analysis

The recovery of hindlimb locomotor function was evaluated by the BMS method which measures hind-limb joint activities, trunk position and stability, coordination of front and rear limbs, paw placement, toe clearance, and tail position. Mice were placed in an open field and activities were recorded by two investigators blinded to the treatment

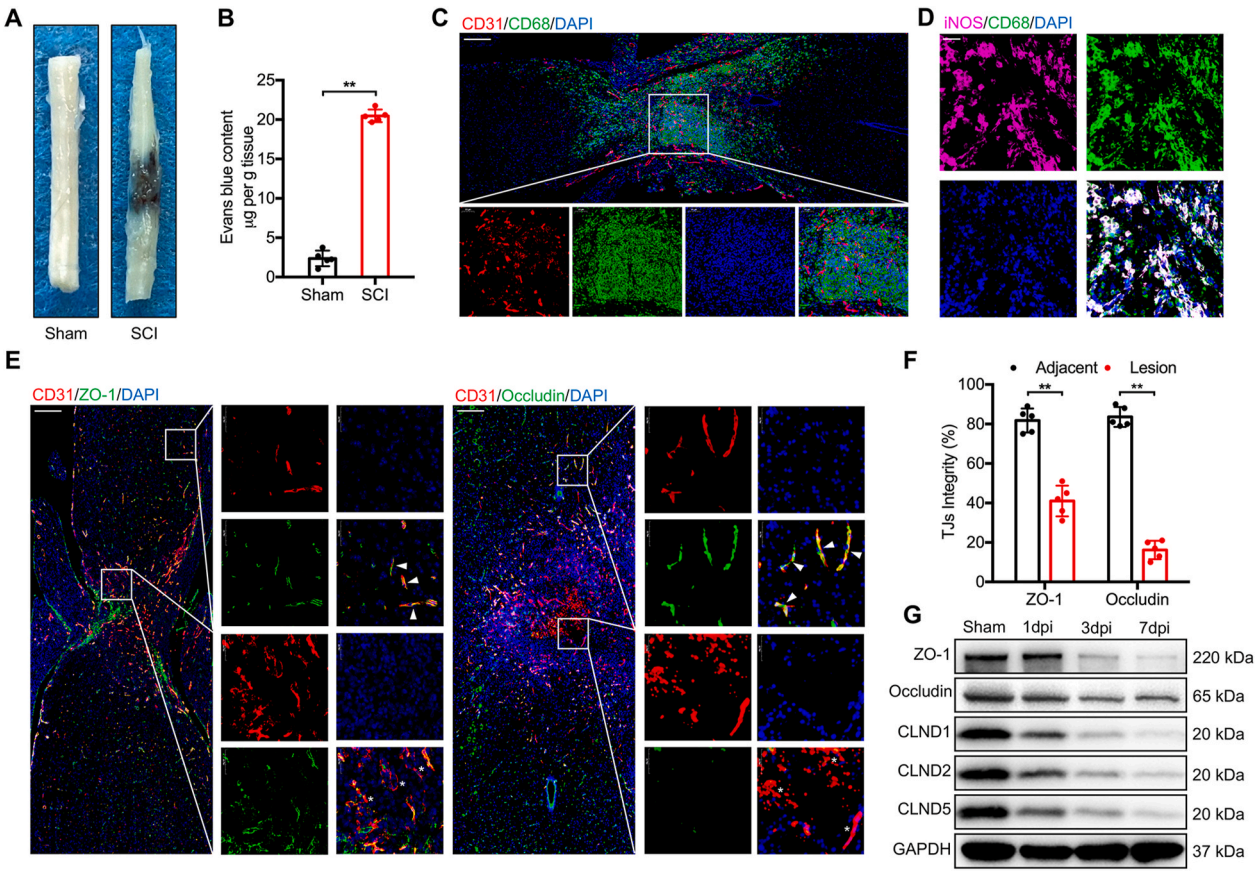

Fig. 1. BSCB breakdown along with macrophages infiltration and TJs disruption after SCI. (A) Representative images of spinal cord after EB injection at day 7 after SCI. (B) Quantification of EB content in spinal cord. (C) Representative double-immunostaining of CD31 and CD68 in the injured spinal cord at day 7 post-injury (Scale bar = 200 μm). (D) Co-immunostaining of CD68 and iNOS in SCI lesion at day 7 post-injury (Scale bar = 100 μm). (E–F) Representative co-immunostaining and quantification of CD31 and TJs markers in the injured spinal cord at day 7 post-injury, with the adjacent area and lesion enlarged (arrows represent vessels with TJs and asterisks represent vessels without TJs. Scale bar = 200 μm). (G) Expression levels of spinal TJs proteins were examined by western blot at indicated time after SCI. **P < 0.01.

group. The scores were measured before surgery and at 1, 3, 7, 14, 21, and 28 days after SCI.

2.15.2. Footprint analysis

Footprint analysis was performed to access the gait and motor coordination at day 28 post-injury. The front and rear paws of mice were brushed with blue and red dyes, respectively, and they were encouraged to walk in a straight line on a paper-lined runway. Footprints were then scanned for quantitative analysis of stride length. At least 5 steps from each side were measured per mouse.

2.15.3. Swimming test

A swimming test was carried out to evaluate the motor function recovery post SCI. Mice were placed in a water-filled tank and trained to swim from one side to the other side. Forelimb dependency, hindlimb movement and alternation, body angle, and trunk stability were recorded and evaluated based on the Louisville Swim Scale. Each mouse was tested twice and mean score was taken as final score.

2.15.4. Electrophysiology testing

Electrophysiology testing was performed to examine motor-evoked potentials (MEPs) at day 28 after SCI. After anesthetizing the mice, a stimulation electrode was placed on rostral ends of exposed spinal cord, and a recording electrode was inserted into the biceps femoris flexor cruris at a depth of 1.5 mm. The reference electrode was placed at distal tendon of the hind limb muscle, and the grounding line was placed subcutaneously. A single square wave (0.5 mA, 0.5 ms, 1 Hz) was applied to induce MEPs, and peak-to-peak amplitudes were calculated to evaluate hind limb nerve conduction function.

2.16. Evaluation of BSCB permeability

The BSCB permeability was measured by Evans blue (EB, Sigma) dye extravasation method. EB dye (2% in saline, 200 μL) was administered at 7 days via i.v. 3 h before the mice were executed. The spinal cord lesion was then removed and homogenized in 50% trichloroacetic acid solution diluted 1:2 in ethanol. Following incubation at 60 °C for 24 h and centrifugation at 10000*g* for 10 min, supernatants were collected and the fluorescence was quantified using a spectrophotometer at 620 nm excitation and 680 emission.

2.17. Statistical analysis

The statistical analysis was conducted using GraphPad Prism 8.0 (GraphPad Software Inc., USA). Data among two groups were compared by Student's t-test, and multivariate analysis was performed using the one-way or two-way ANOVA test. Results were shown as mean ± standard deviation (SD) and differences were considered significant at *P* value < 0.05.

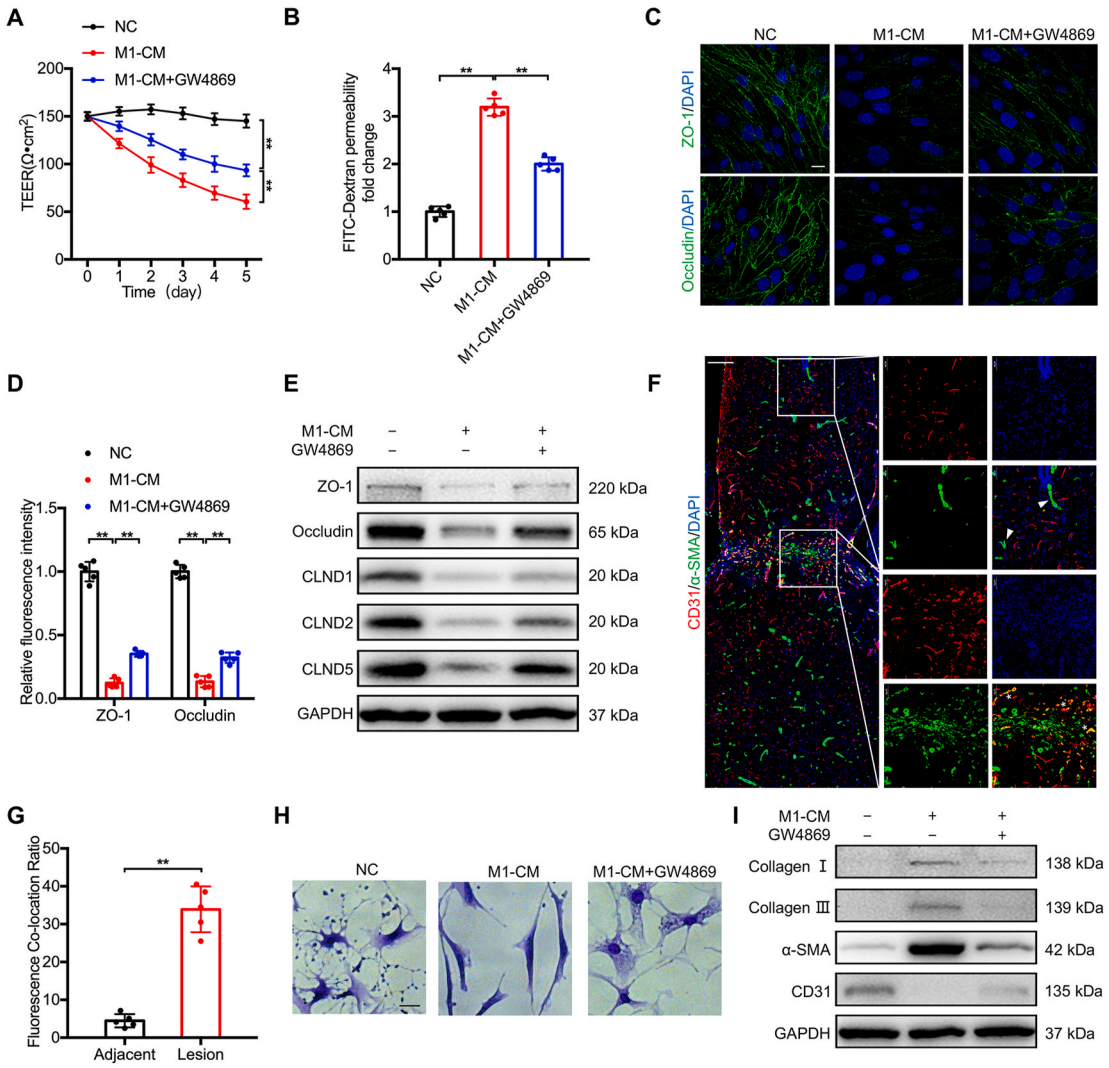

Fig. 2. M1-BMDMs-derived exosomes aggravate EndoMT in bEnd.3 cells *in vitro*. (A) TEER value and (B) FITC-Dextran leak were used to determine barrier function of bEnd.3 cells after treatment of M1-CM with or without GW4869. (C–D) Immunofluorescence detection and quantification of ZO-1 and Occludin in bEnd.3 cells (Scale bar = 10 μm). (E) Expression levels of TJs protein determined by western blot in indicated groups. (F–G) Representative co-immunostaining and quantification of CD31 and α-SMA in the injured spinal cord at day 7 post-injury (Arrows represent vessels without EndoMT and asterisks represent vessels with EndoMT. Scale bar = 200 μm). (H) Morphology of bEnd.3 cells in indicated groups (Scale bar = 50 μm). (I) Protein levels of EndoMT markers and CD31 in indicated groups were determined by western blot. $^{**}P < 0.01$.

3. Results

3.1. BSCB breakdown along with macrophages infiltration and TJs disruption after SCI

Following SCI, integrity of BSCB was disrupted, as shown in Fig. 1A and B, EB dye was clearly observed in SCI lesion, but not in sham group, and its content in the spinal cord was significantly increased in SCI group as well. Moreover, along with the destruction of BSCB, we found a large number of macrophages infiltrated around vessels in the injured area (Fig. 1C), which were predominately M1-polarized, indicated with $CD68^+$ and $iNOS^+$ (Fig. 1D). In contrast, the M2-polarized macrophages (indicated with $CD68^+$ and $ARG1^+$) were far less than M1 macrophages (Figs. S1A–B). Although both the mRNA levels of iNOS and CD206 (an M2 marker) were increased in the early 7 days after SCI, the iNOS upregulation is much more significant than CD206 (Fig. S1C). These data suggest that M1 polarization of infiltrated macrophages plays a dominant role in the early stage after SCI. Furthermore, significant angiogenesis was observed in the lesion after SCI, which might be induced by the hypoxia microenvironment; however, fluorescence staining of TJs and vessels demonstrated less co-location of ZO-1 and Occludin with CD31 in the injured area compared with the non-injured area (Fig. 1E and F). This means that newborn vessels had problems in TJs assembly; in other words, they were highly permeable. In addition, the TJs protein levels significantly decreased with time after SCI (Fig. 1G). Given that there exists crosstalk between infiltrated M1-polarized macrophages and vessels in the lesion area following SCI, we hypothesized that M1-polarized macrophages may exert important effects on vascular endothelial cells and impair BSCB integrity following SCI.

M1-BMDMs-derived exosomes aggravate EndoMT in bEnd.3 cells *in vitro*.

Based on above results. we next evaluated the effects of M1-BMDMs on bEnd.3 cells *in vitro*. BMDMs were firstly separated, then LPS was used to induce M1 polarization (Fig. S2). As expected, conditioned medium of M1-BMDMs (M1-CM) significantly decreased the TEER value of bEnd.3 cells (Fig. 2A) and increased the FITC-dextran permeability (Fig. 2B). Moreover, fluorescent staining of TJs proteins demonstrated that treatment with M1-CM markedly decreased expression of ZO-1 and Occludin in the bEnd.3 cell membranes (Fig. 2C and D). Considering

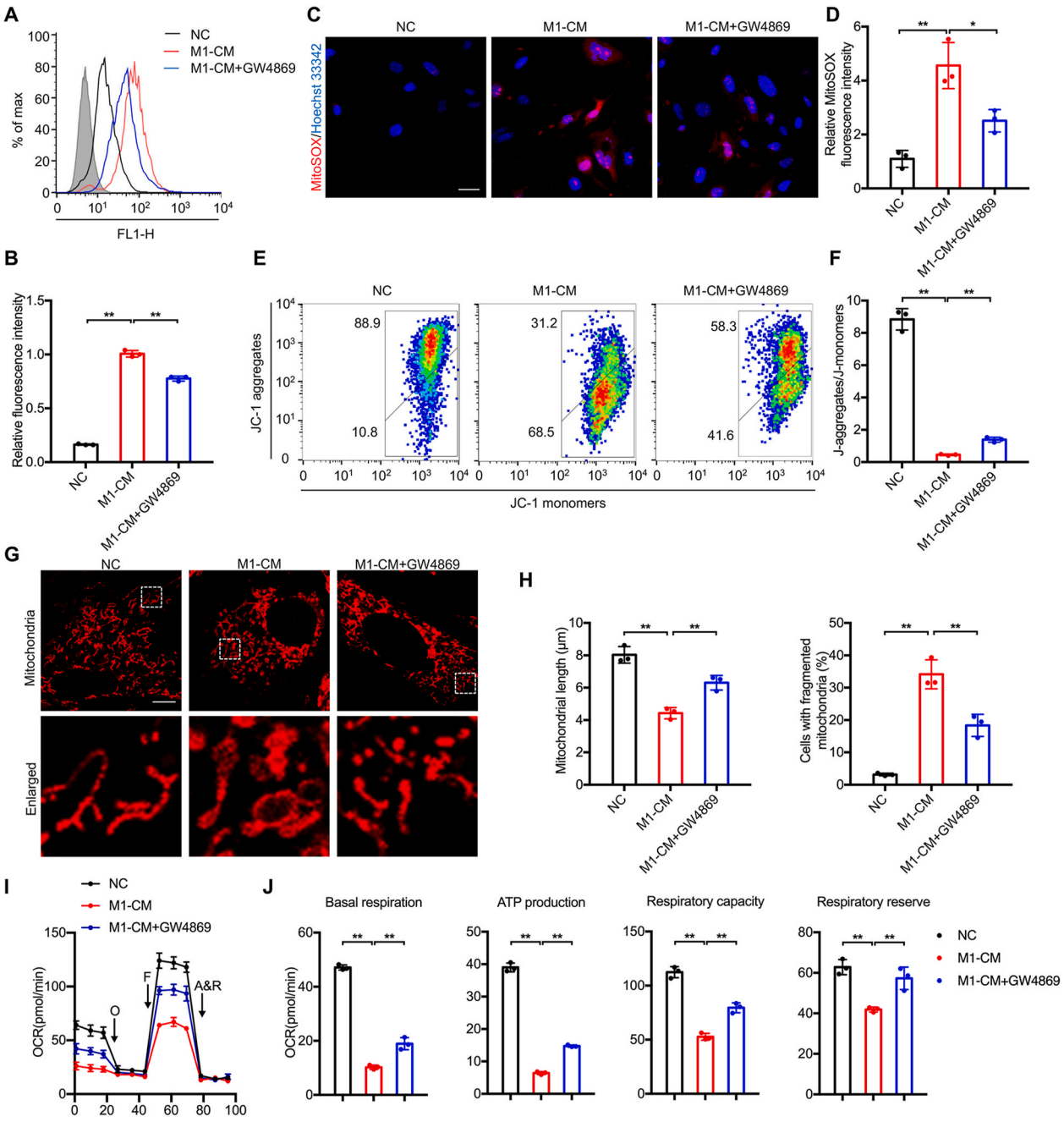

Fig. 3. M1-BMDMs-derived exosomes upregulate ROS level and impair mitochondrial function of bEnd.3 cells *in vitro*. (A–B) Detection and quantification of ROS levels in bEnd.3 cells by flow cytometry in indicated groups. (C–D) Immunofluorescence microscopy detection and quantification of MitoSOX in indicated groups (Scale bar = 50 μm). (E–F) Mitochondrial potential was determined and quantified by JC-1 aggregates/JC-1 monomers by flow cytometry in indicated groups. (G–H) Representative images of mitochondrial morphology and quantification of mitochondrial length and percentage of cells with fragmented mitochondria in indicated groups (Scale bar = 5 μm). (I–J) OCR was used to evaluate mitochondrial functions of bEnd.3 cells. *P < 0.05, **P < 0.01.

exosomes are involved in paracrine effect between two cells to mediate cell-to-cell communication, and to further investigate whether M1-BMDMs wreck TJs of vascular endothelial cells through exosomes, GW4869 (an exosomal secretion inhibitor) was used to pretreat M1-BMDMs. We found that addition of GW4869 partly reversed M1-CM-induced TEER value decline (Fig. 2A) and FITC-dextran permeability increase (Fig. 2B); fluorescence intensity decrease of TJs proteins was reversed by GW4869 as well (Fig. 2C and D). Correspondingly, expression levels of TJs proteins demonstrated similar results (Fig. 2E).

Interestingly, through co-staining of EndoMT marker α-smooth muscle actin (α-SMA) with CD31 in spinal cord sections, we found more co-location in injured lesions than in uninjured areas (Fig. 2F and G), which indicated EndoMT of vascular endothelial cells in lesion area following SCI. Indeed, M1-CM significantly altered cell morphology of bEnd.3 cells with reduced branches and elongated cell soma *in vitro* (Fig. 2H). Additionally, exposure to M1-CM markedly attenuated CD31 expression and strongly enhanced expression of EndoMT markers collagen I, III and α-SMA in bEnd.3 cells (Fig. 2I). However, administration of GW4869 could partly reverse these effects. Taken together, we concluded that exosomes may mediate the interaction between macrophages and vascular endothelial cells and may be responsible for macrophage-induced EndoMT in vascular endothelial cells.

M1-BMDMs-derived exosomes upregulate ROS level and impair mitochondrial function of bEnd.3 cells *in vitro*.

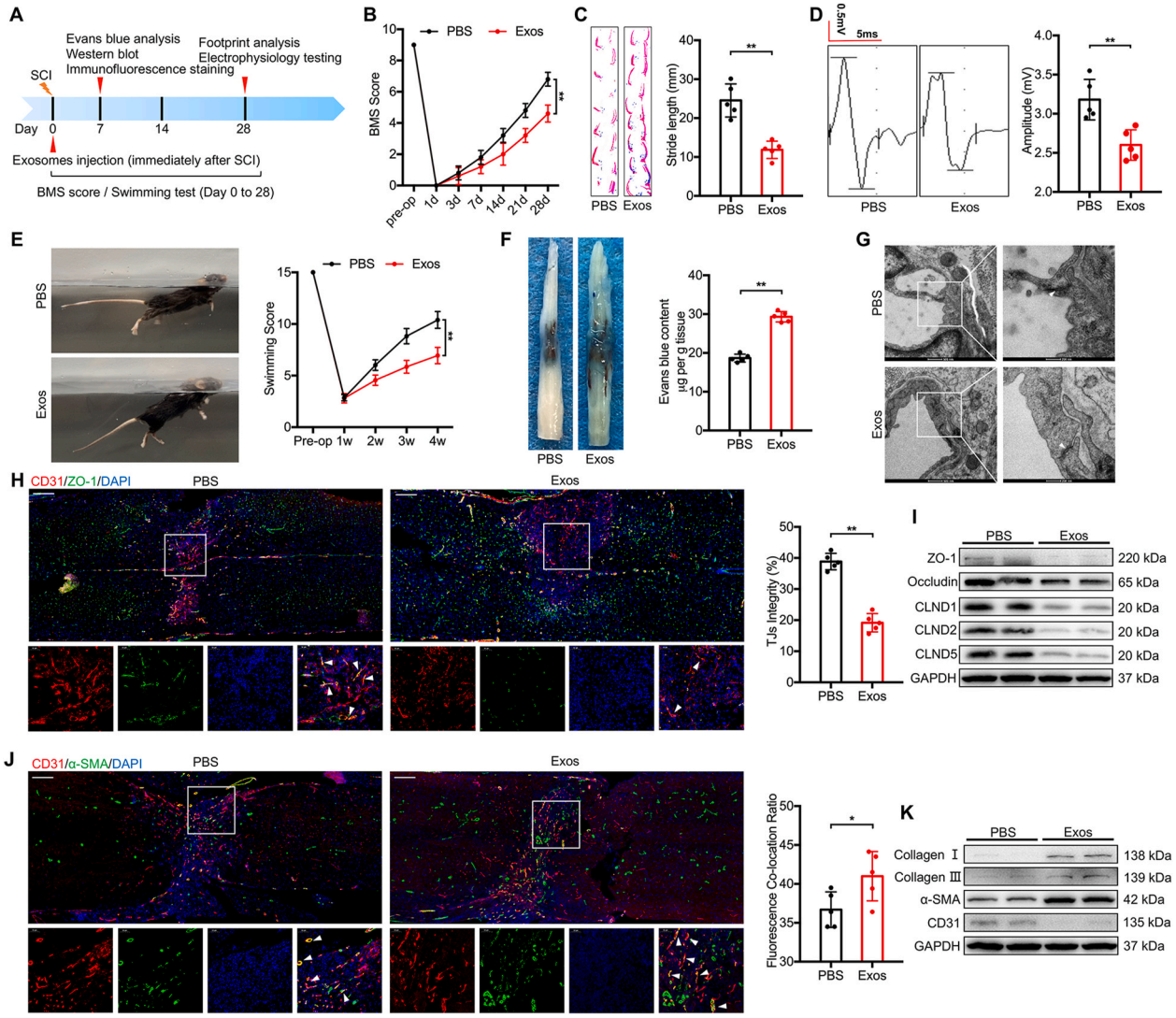

Fig. 4. Exosomes derived from M1-BMDMs hinder motor function recovery and disrupt BSCB after SCI *in vivo*. (A) The experimental scheme for exosomes injection after SCI and data presented in panels B–K. (B) BMS was used to functionally grade mice in different groups up to 28 days post-injury. (C) Representative footprints and stride length analysis of mice at day 28 post-injury. (D) Representative MEPs and amplitude analysis of mice 28 days post-injury. (E) LSS score was used to functionally grade mice up to 28 days post-injury. (F) Representative images of spinal cord after EB injection at day 7 post-injury and EB content quantification. (G) TEM was used to observe vascular TJs morphology in mice administered with PBS or M1-Exos (Arrows represent TJs). (H) Representative co-immunostaining and quantification of CD31 and ZO-1 in the injured spinal cord at day 7 post-injury (Scale bar = 200 μm). (I) Expression of TJs proteins in PBS and M1-Exos groups at day 7 post-injury was determined by western blot. (J) Representative co-immunostaining and quantification of CD31 and α-SMA in the injured spinal cord at day 7 post-injury (Arrows represent vessels with EndoMT. Scale bar = 200 μm). (K) Expression of EndoMT markers and CD31 in PBS and M1-Exos groups at day 7 post-injury was determined by western blot. *P < 0.05, **P < 0.01.

It has been reported that ROS are associated with BSCB disruption, and modulating ROS level plays a crucial role in promoting functional recovery after CNS injury [31]. Based on previous results, we investigated the relationship between M1-BMDMs and ROS in bEnd.3 cells. Flow cytometry analysis demonstrated that M1-CM treatment markedly increased ROS level in bEnd.3 cells and that GW4869 could partly reverse this increase (Fig. 3A and B). In addition, incubation with M1-CM significantly increased mitochondrial superoxide level, which was partly abolished by GW4869 as well (Fig. 3C and D). As shown by JC-1 staining, there was a significant decrease of mitochondrial potential following M1-CM addition, and GW4869 partly restored the mitochondrial potential (Fig. 3E and F). Clearly, M1-CM treatment shortened mitochondrial length and made them swell, and percentage of cells with fragmented mitochondria was markedly increased as well. Nevertheless, GW4869 could partly reverse mitochondrial morphological changes (Fig. 3G and H). Moreover, M1-CM exposure markedly decreased OCR which is a biomarker of oxidative phosphorylation (Fig. 3I). Also, basal respiration, ATP production, respiration capacity, and respiration reverse in bEnd.3 cells were significantly decreased upon M1-CM addition, and these effects were also partly mitigated by GW4869 (Fig. 3J).

Exosomes derived from M1-BMDMs hinder motor function recovery and disrupt BSCB after SCI *in vivo*.

To further investigate the role of macrophages in SCI microenvironment and their potential effects on vascular endothelial cells, exosomes derived from M1-BMDMs (M1-Exos) were then extracted and identified (Fig. S3). Following exosomes injection immediately after SCI, a series of behavioral assessment was performed at indicated time (Fig. 4A). The BMS behavioral analysis demonstrated that M1-Exos injection induced a lower score of hindlimb locomotor function after SCI (Fig. 4B). The footprint analysis, electrophysiology testing and swimming test showed similar results, as M1-Exos administration resulted in

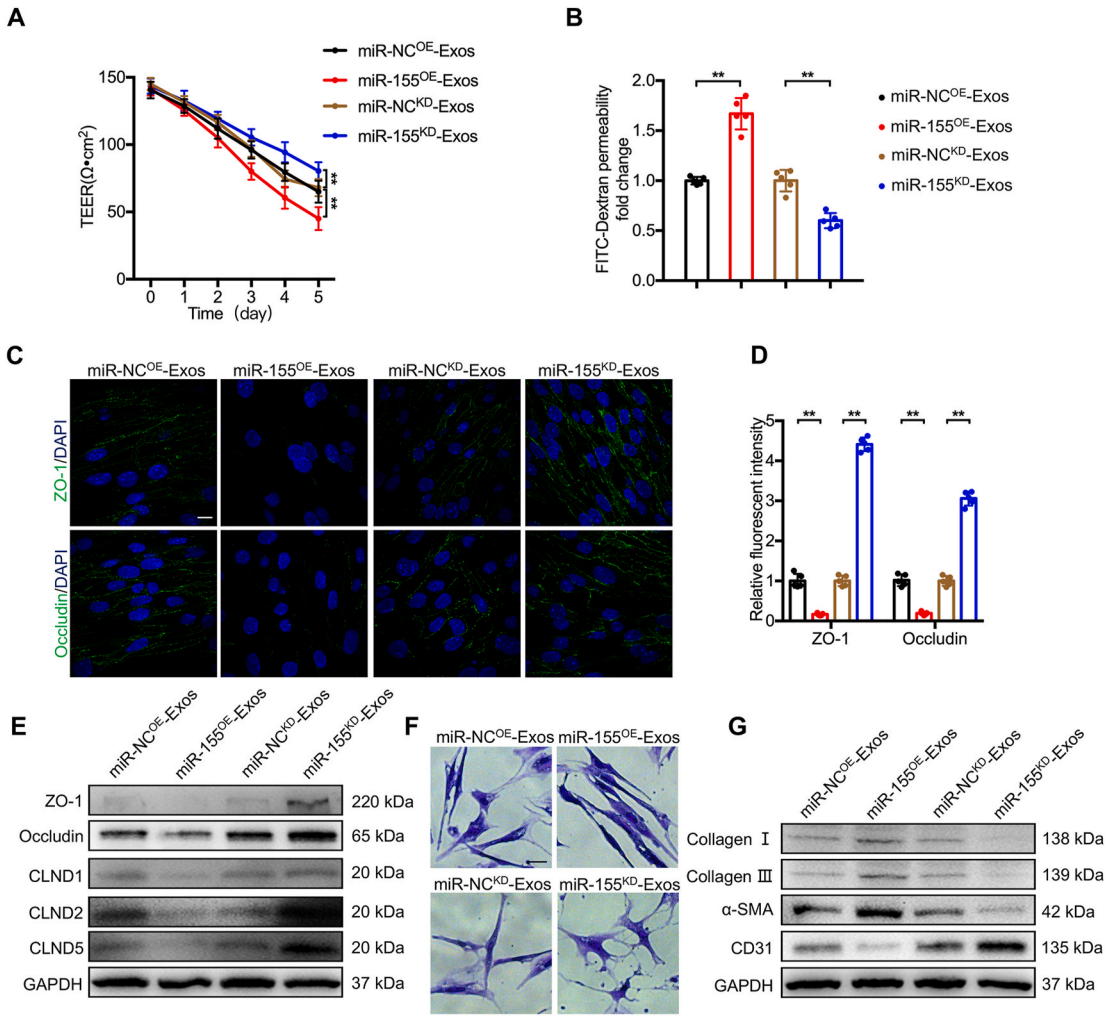

Fig. 5. M1-Exos aggravate EndoMT in bEnd.3 cells by delivering miR-155 *in vitro*. (A) TEER value and (B) FITC-Dextran leak was used to evaluate the effect of exosomal miR-155 on barrier function of bEnd.3 cells. (C–D) Representative immunostaining images and quantification of ZO-1 and Occludin fluorescence intensity in indicated groups (Scale bar = 10 μm). (E) Expression of TJs proteins was determined by western blot. (F) Representative morphological images of bEnd.3 cells in indicated groups (Scale bar = 50 μm). (G) Expression of EndoMT markers and CD31 was determined by western blot. **P < 0.01.

shorter stride length (Fig. 4C), lower MEPs amplitude (Fig. 4D), more inclined body angle, and more pendent tail (Fig. 4E). The EB extravasation assay further demonstration that more EB dye leaked into interstitial space (Fig. 4F) in the M1-Exos-treated group, and electron density of vascular TJs under TEM was much lower than PBS group, the gap between two endothelial cells was more apparent as well (Fig. 4G). In addition, the fluorescent intensity of vascular ZO-1 in spinal lesions was significantly attenuated following M1-Exos injection (Fig. 4H); expression levels of TJs proteins were markedly downregulated as well (Fig. 4I). Moreover, we found more co-location of α-SMA with CD31 in lesion area after M1-Exos administration (Fig. 4J); in addition, the protein levels of collagen I, III and α-SMA were upregulated and CD31 expression was reduced (Fig. 4K). The above results indicated that M1-Exos might induce EndoMT to aggravate BSCB breakdown and hinder motor function recovery after SCI.

miR-155 is upregulated in M1-BMDMs and can be transferred to bEnd.3 cells by exosomes.

Bioinformatics analysis of GSE33453 and GSE49330 revealed that only miR-155 is upregulated in both LPS-treated macrophages and microglia compared with unstimulated macrophages and microglia (Figs. S4A–C), which was further confirmed by qRT-PCR in LPS-induced BMDMs (Fig. S4D). Notably, miR-155 expression was significantly enhanced in M1-Exos and M1-Exos-treated bEnd.3 cells as well (Figs. S4E–F), indicating that miR-155 could be transferred from BMDMs to bEnd.3 cells through exosomes.

M1-Exos aggravate EndoMT in bEnd.3 cells by delivering miR-155 *in vitro*.

To investigate the role of exosomal miR-155 in the deterioration of M1-Exos-mediated BSCB disruption after SCI, miR-155 overexpression (miR-155^{OE}) and knockdown (miR-155^{KD}) BMDMs were constructed and exosomes were then isolated to treat bEnd.3 cells. Transfection efficiency is shown in Fig. S5A. As expected, a significant increase of miR-155 expression and a marked decrease of miR-155 expression were observed in exosomes derived from miR-155^{OE} (miR-155^{OE}-Exos) and miR-155^{KD} (miR-155^{KD}-Exos) BMDMs, respectively, compared with the negative control (Fig. S5B). Furthermore, miR-155 expression in target bEnd.3 cells was significantly upregulated by treatment with miR-155^{OE}-Exos compared with miR-NC^{OE}-Exos, while it was downregulated by treatment with miR-155^{KD}-Exos compared with miR-NC^{KD}-Exos (Fig. S5C). Several functional experiments were then carried out. As shown in Fig. 5A and B, there was a dramatic decrease in TEER value and an increase in FITC-dextran permeability in the miR-155^{OE}-Exos group, while an opposite result was observed in miR-155^{KD}-Exos group. Indeed, fluorescent intensity of ZO-1 and Occludin was markedly decreased by addition of miR-155^{OE}-Exos, while miR-155^{KD}-Exos treatment strongly enhanced ZO-1 and Occludin expression (Fig. 5C and D). Furthermore, expression of TJs proteins detected by western blot demonstrated similar results with those discussed above (Fig. 5E). In addition,

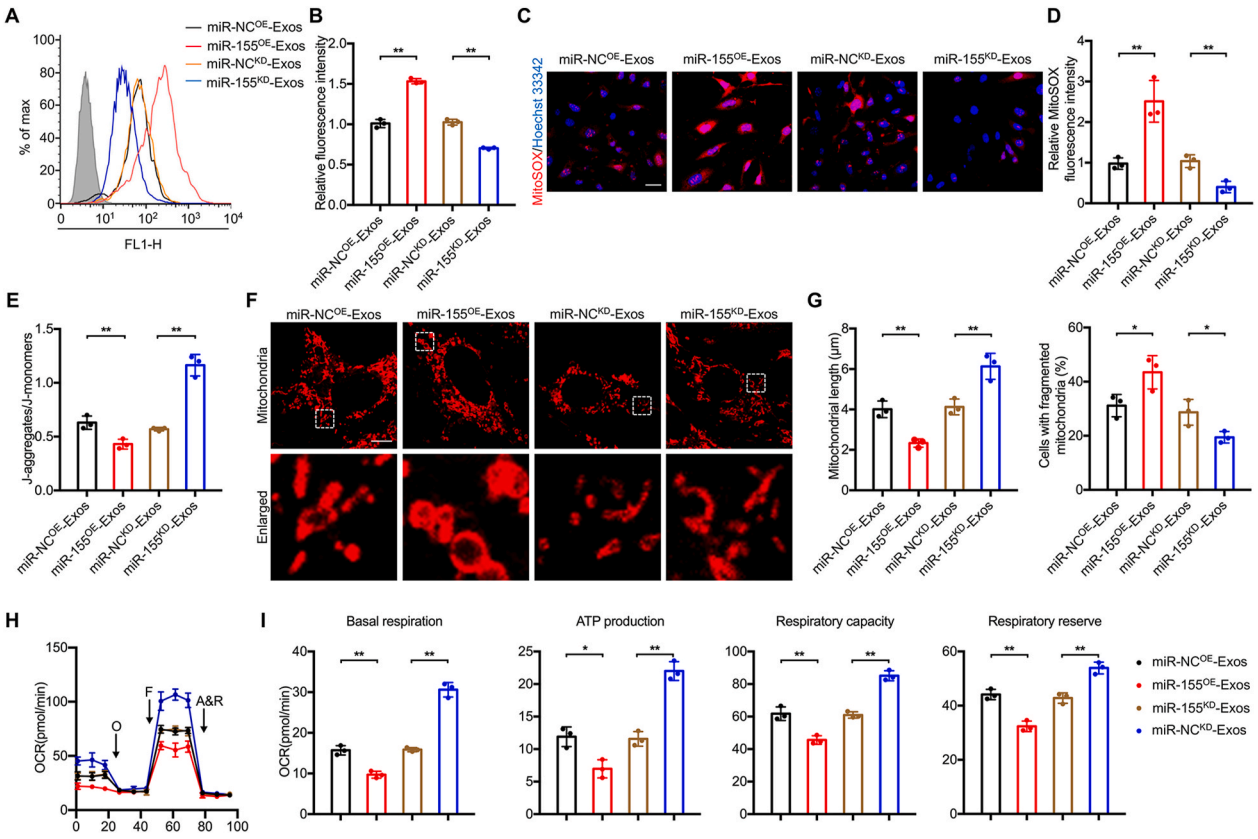

Fig. 6. M1-Exos upregulate ROS level and impair mitochondrial function of bEnd.3 cells by delivering miR-155 *in vitro*. (A–B) Detection and quantification of ROS levels in bEnd.3 cells by flow cytometry. (C–D) Immunofluorescence detection and quantification of MitoSOX in bEnd.3 cells (Scale bar = 50 μm). (E) Quantification of mitochondrial potential by JC-1 aggregates/JC-1 monomers. (F–G) Representative images of mitochondrial morphology and quantification of mitochondrial length and percentage of cells with fragmented mitochondria (Scale bar = 5 μm). (H–I) OCR was used to evaluate the effects of exosomal miR-155 on mitochondrial functions. *P < 0.05, **P < 0.01.

administration of miR-155^{OE}-Exos promoted cell morphology transformation with less branches and longer soma. The results were opposite after treatment with miR-155^{KD}-Exos (Fig. 5F). Moreover, protein levels of collagen I, III and α-SMA were upregulated and level of CD31 was downregulated after miR-155^{OE}-Exos exposure, while miR-155^{KD}-Exos administration exerted opposite effects (Fig. 5G). The above results revealed that exosomal miR-155 plays a crucial role in promoting EndoMT of bEnd.3 cells *in vitro*.

M1-Exos upregulate ROS level and impair mitochondrial function of bEnd.3 cells by delivering miR-155 *in vitro*.

We next investigated the relationship between exosomal miR-155 and mitochondrial function in bEnd.3 cells. We found that treatment with miR-155^{OE}-Exos upregulated ROS level (Fig. 6A and B), mitochondrial superoxide level (Fig. 6C and D), and mitochondrial potential (Fig. 6E) compared with miR-NC^{OE}-Exos administration; miR-155^{KD}-Exos administration, however, demonstrated the opposite results (Fig. 6A–E). Furthermore, miR-155^{OE}-Exos administration induced much more swelling and shorter morphology in mitochondria with a higher percentage of cells with fragmented mitochondria, while miR-155^{KD}-Exos administration could alleviate mitochondrial swelling (Fig. 6F and G). In addition, there was a clear decline of OCR, basal respiration, ATP production, respiration capacity, and respiration reverse in mitochondrial function after miR-155^{OE}-Exos administration, while miR-155^{KD}-Exos treatment alleviated oxidative respiratory dysfunction (Fig. 6H and I). Taken together, these results revealed that upregulated exosomal miR-155 could result in excessive ROS production and mitochondrial dysfunction.

miR-155 negatively regulates SOCS6 expression and activates the NF-κB pathway.

To further explore potential mechanism of exosomal miR-155-induced EndoMT and mitochondrial dysfunction, we focused on the downstream genes of miR-155. Firstly, a total of 84 potential target genes were predicted using an online database of miRNA targets. SOCS6 is one of the downstream mRNAs with a 3' untranslated region (3'UTR) that might bind to miR-155 (Fig. 7A). By combining the GSE49329 and GSE49330 databases, we found that miR-155 expression is negatively correlated with SOCS6 expression (Fig. 7B). To further confirm that SOCS6 3'UTR is a direct target of miR-155, wild type (WT) and mutant (MUT) sequences of SOCS6 3'UTR were constructed based on the predicted binding site (Fig. 7C) and co-transfected with miR-155 sequence into bEnd.3 cells. The luciferase report assay demonstrated that miR-155 overexpression significantly decreased luciferase activity when co-transfected with WT-3' UTR of SOCS6 compared with control, whereas no inhibitory effect of miR-155 on luciferase activity was observed when co-transfected with MUT-3' UTR of SOCS6 (Fig. 7D). The qRT-PCR and western blot assay further revealed that miR-155 overexpression resulted in lower expression of SOCS6, while miR-155 knockdown upregulated SOCS6 mRNA and protein levels (Fig. 7E and F). Interestingly, through Gene Ontology (GO) analysis of the total 84 miR-155-target genes, we found that miR-155 could negatively regulate cell-cell adhesion and participate in regulation of fibroblast proliferation, which is consistent with our aforementioned results (Fig. 7G). It should be mentioned that miR-155 may mediate the NF-κB signaling pathway according to GO analysis (Fig. 7G), and miR-155 overexpression markedly increased the p65 protein level in cytoplasm and nucleus, while miR-155 knockdown exerted opposite effects (Fig. 7H).

SOCS6 suppresses NF-κB signaling pathway by ubiquitylating and degrading p65.

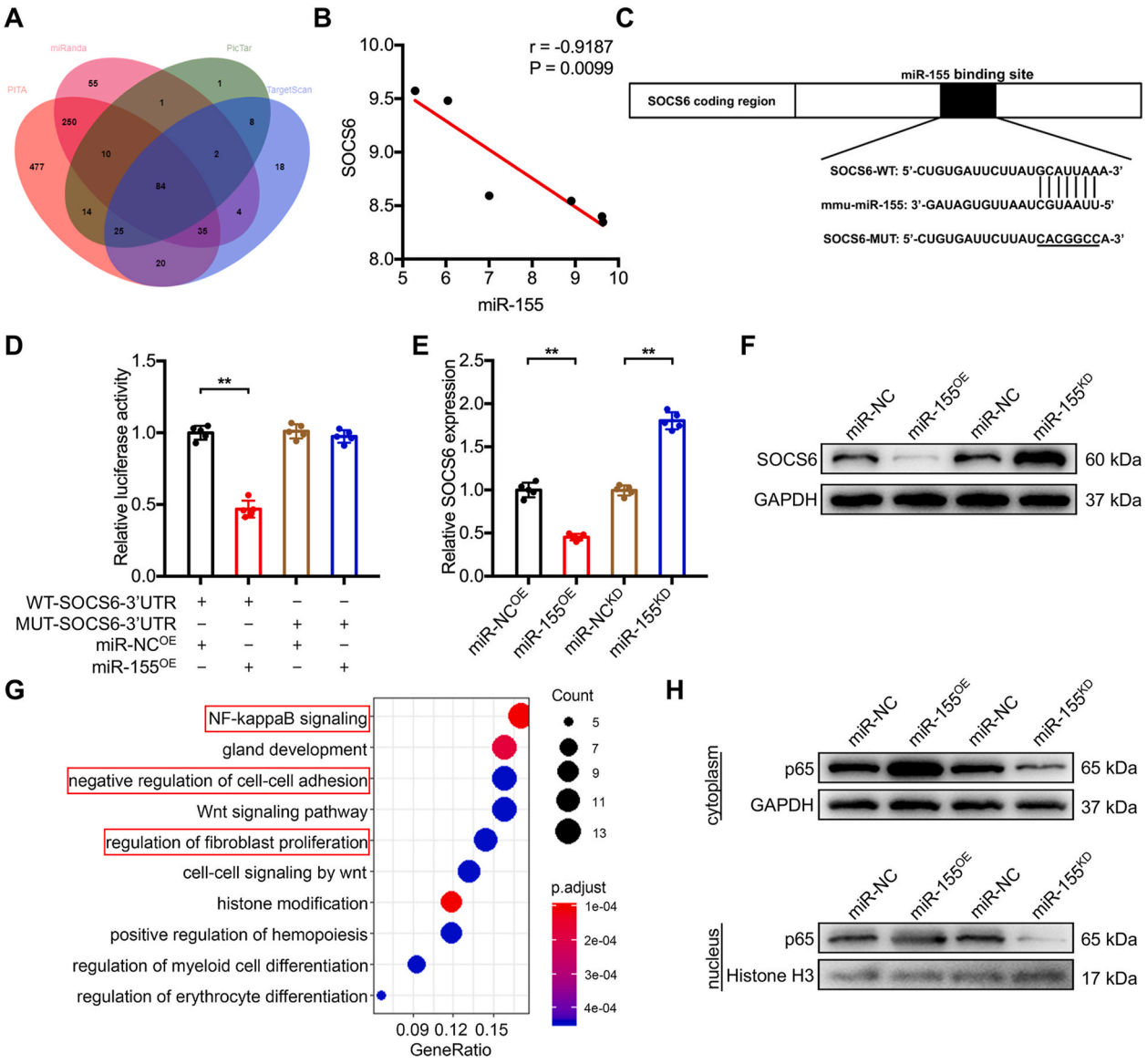

Fig. 7. miR-155 negatively regulates SOCS6 expression and activates the NF-κB pathway. (A) Predicted target genes of miR-155. (B) Correlation analysis of miR-155 and SOCS6 expression. (C) miR-155 regulated SOCS6 by directly targeting the 3'-UTR. (D) Luciferase report assay was performed to confirm SOCS6 is the target gene of miR-155. (E) The mRNA level of SOCS6 in bEnd.3 cells after treatment with miR-155^{OE}-Exos and miR-155^{KD}-Exos. (F) The protein level of SOCS6 in bEnd.3 cells after treatment with miR-155^{OE}-Exos and miR-155^{KD}-Exos. (G) The GO enrichment analysis of target genes of miR-155. (H) The protein level of p65 in cytoplasm and nucleus after treatment with miR-155^{OE}-Exos and miR-155^{KD}-Exos. **P < 0.01.

Given that miR-155 negatively regulated SOCS6 expression and activated the NF-κB signaling pathway through enhancing p65 expression in cytoplasm and nucleus, we next investigated the potential interaction between SOCS6 and p65. It has been shown that SOCS6 as an E3 ubiquitin ligase mediates protein proteolysis; to further explore whether SOCS6 ubiquitylates p65 and induces its degradation, we carried out a series of experiments. Firstly, we overexpressed or down-regulated SOCS6 in bEnd.3 cells and found that p65 expression was negatively correlated with the SOCS6 level (Fig. 8A). The 3D docking analyzed by Discovery Studio™ also demonstrated SOCS6 might interact with p65 (Fig. 8B). Moreover, fluorescence co-location assay demonstrated that SOCS6 and p65 are co-located in cytoplasm (Fig. 8C and D), and the Co-IP assay further revealed interaction between SOCS6 and p65 (Fig. 8E). Notably, addition of 10 μM proteasome MG132 could partly reverse the inhibitory effects of SOCS6 overexpression on p65 protein level (Fig. 8F). Meanwhile, silence of SOCS6 significantly retarded the degradation rate of endogenous p65 in the presence of 100 μg/mL cycloheximide, an inhibitor of protein translation, while overexpressing SOCS6 markedly accelerated p65 degradation (Fig. 8G). Finally, an ubiquitylation assay was performed to validate whether SOCS6 induces p65 destabilization via proteasomal degradation. It was found that overexpressing SOCS6 increased p65 polyubiquitination in bEnd.3 cells, while SOCS6 silence showed an opposite result (Fig. 8H). Taken together, these results revealed that SOCS6 could bind to p65 and induce its polyubiquitination and proteasomal degradation.

M1-Exos aggravate EndoMT in bEnd.3 cells through miR-155/SOCS6/p65 axis.

To explore the role of exosomal miR-155/SOCS6/p65 axis in M1-Exos-induced EndoMT, we performed a series of loss- and gain-of-function experiments *in vitro*. Firstly, we administered miR-NC^{OE}-Exos and miR-155^{OE}-Exos into SOCS6-overexpressed bEnd.3 cells and miR-NC^{KD}-Exos and miR-155^{KD}-Exos into SOCS6-knockdown bEnd.3 cells. We found that SOCS6 overexpression partly reversed the TEER value decrease and FITC-Dextran permeability increase induced by miR-NC^{OE}-Exos or miR-155^{OE}-Exos (Fig. 9A and B). Fluorescence intensity of ZO-1 and Occludin further revealed that SOCS6 overexpression significantly

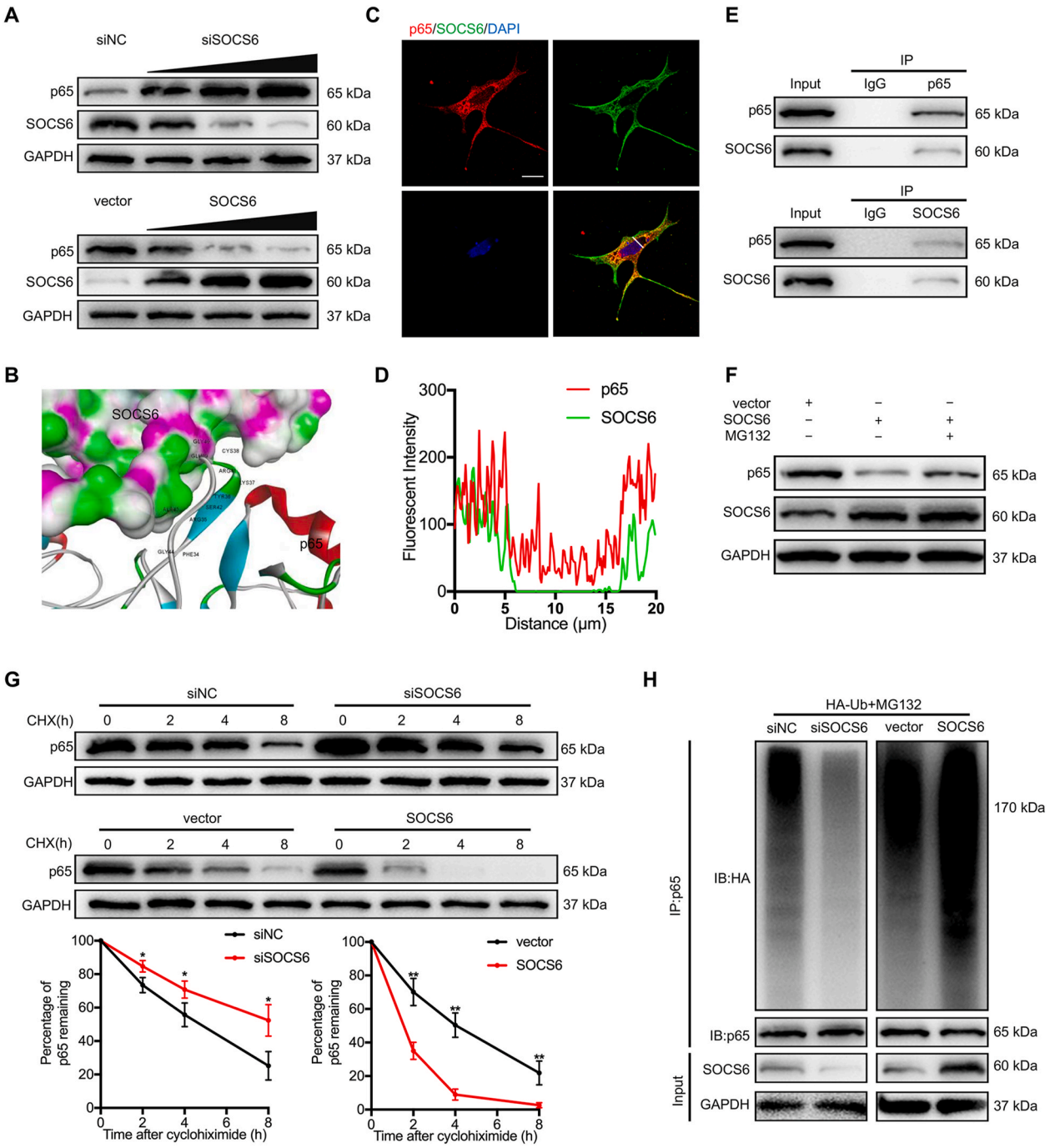

Fig. 8. SOCS6 suppresses the NF-κB signaling pathway by ubiquitylating and degrading p65. (A) The protein level of p65 in bEnd.3 cells after SOCS6 knockdown and overexpression. (B) 3D mocking was used to analyze interaction between SOCS6 and p65. (C–D) Immunofluorescence co-location of p65 and SOCS6 in cytoplasm (Scale bar = 10 μm). (E) Co-IP was performed to analyze interaction between SOCS6 and p65. (F) Western blot analysis of p65 and SOCS6 in bEnd.3 cells over-expressed SOCS6, with or without addition of proteasome inhibitor MG132. (G) The protein level of p65 in SOCS6-overexpressed or -depleted bEnd.3 cells in the presence of cycloheximide (100 μg/mL) for indicated time. Quantification of p65 is shown. (H) Co-IP assay was conducted with anti-p65 antibody, followed by the detection of ubiquitin-conjugated p65 with anti-HA antibody. *P < 0.05, **P < 0.01.

reversed TJs disruption which caused by miR-NC^{OE}-Exos or miR-155^{OE}-Exos in bEnd.3 cells (Fig. 9C). Moreover, protein levels of EndoMT markers are consistent with these results, and SOCS6 upregulation could eliminate the upregulation of p65 mediated by miR-NC^{OE}-Exos or miR-155^{OE}-Exos (Fig. 9D). Notably, opposite results were observed when SOCS6 was downregulated after administration of miR-NC^{KD}-Exos or miR-155^{KD}-Exos (Fig. 9E–H).

M1-Exos upregulate ROS level and impair mitochondrial function in bEnd.3 cells through miR-155/SOCS6/p65 axis.

We performed a series of loss- and gain-of-function experiments to investigate the role of miR-155/SOCS6/p65 axis in regulating mitochondrial function. As shown in Fig. 10A–E, SOCS6 overexpression eliminated the increase in ROS level (Fig. 10A and B), mitochondrial superoxide content (Fig. 10C and D), and mitochondrial potential (Fig. 10E) induced by miR-NC^{OE}-Exos or miR-155^{OE}-Exos. Moreover, SOCS6 overexpression significantly alleviated mitochondria swelling and reduced the percentage of cells with fragmented mitochondria after miR-NC^{OE}-Exos or miR-155^{OE}-Exos administration (Fig. 10F and G).

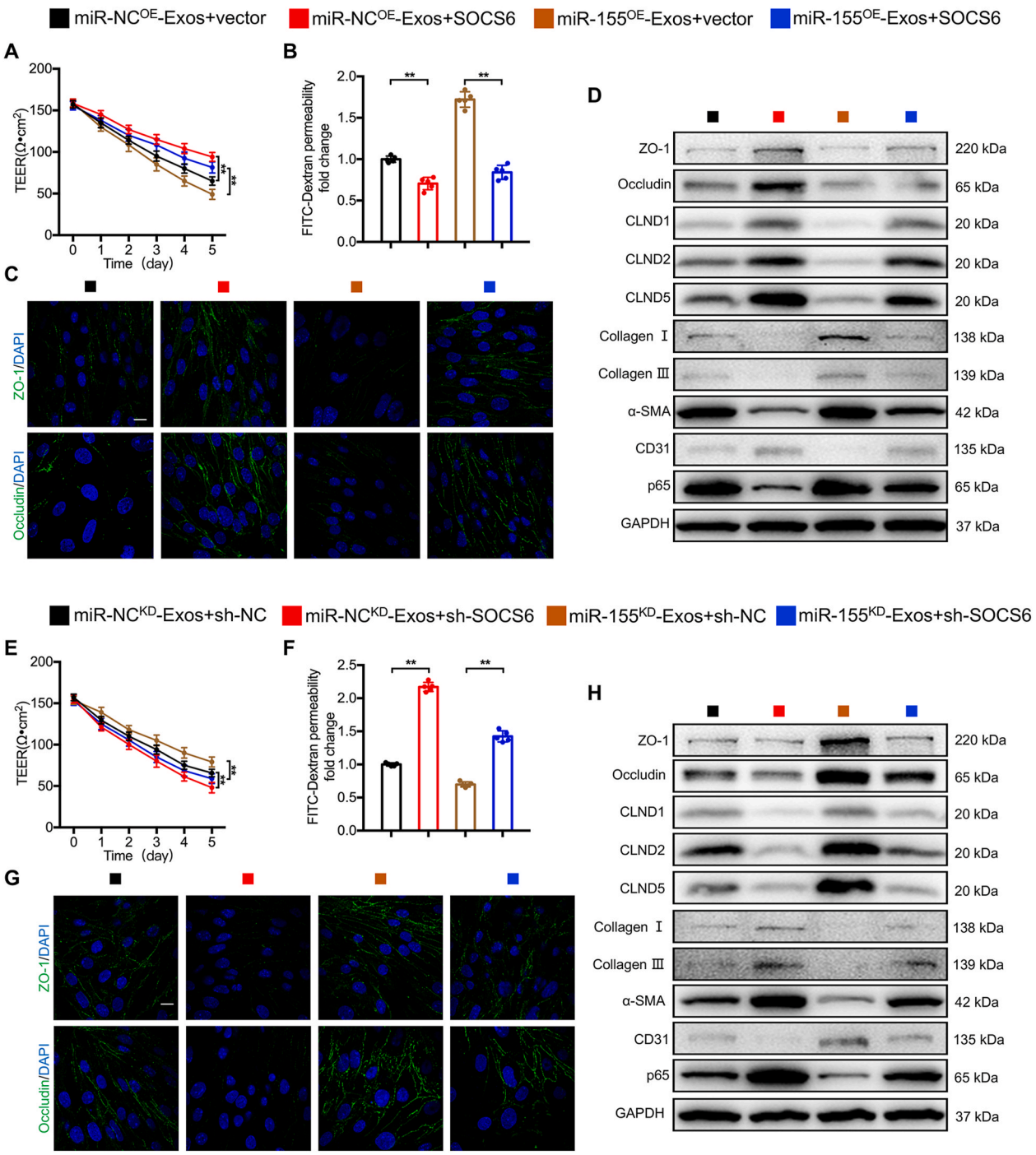

Fig. 9. M1-Exos aggravate EndoMT in bEnd.3 cells through miR-155/SOCS6/p65 axis. (A–H) A series of loss- and gain-of-function experiments *in vitro* was conducted to verify the functional effects of exosomal miR-155/SOCS6/p65 axis on TJs disruption and EndoMT. Rescue experiments for miR-155 overexpression were carried out by ectopic expression of SOCS6, and rescue experiments for miR-155 depletion were performed by SOCS6 depletion. Vascular TJs function was determined by TEER (A and E), FITC-Dextran permeability (B and F), and immunofluorescence staining of ZO-1 and Occludin (C and G, scale bar = 10 μm). (D and H) Levels of TJs proteins and EndoMT markers were determined by western blot. $^{**}P < 0.01$.

Further results indicated that SOCS6 overexpression could rescue the decline of OCR, basal respiration, ATP production, respiration capacity, and respiration reverse impaired by miR-NC^{OE}-Exos or miR-155^{OE}-Exos treatment (Fig. 10H and I). Additionally, opposite results were observed when silencing SOCS6 after administration of miR-NC^{KD}-Exos or miR-155^{KD}-Exos (Fig. 10J-R).

4. Discussion

SCI is an irreversible neurotrauma characterized by several major biological cascades starting with structural or functional disruption of microvessels and BSCB rupture, which results in subsequent spinal edema, neuroinflammation, and neuronal or glial necrosis [3,32]; thus, re-establishment of BSCB is of great benefits for axonal regeneration and motor recovery after SCI [6,33]. Although significant angiogenesis has been observed in injury lesions after SCI, which contributes to SCI

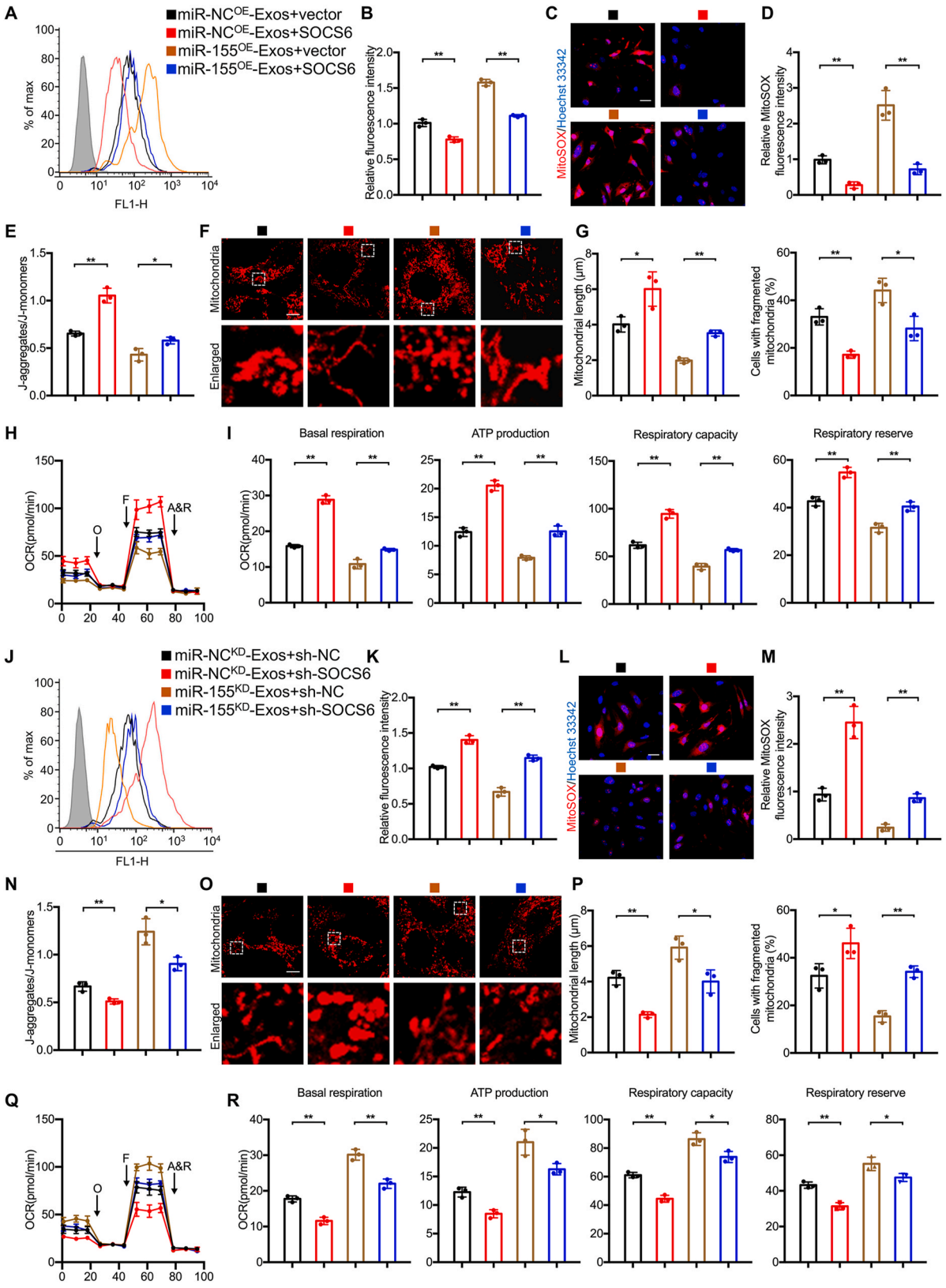

Fig. 10. M1-Exos upregulate ROS level and impair mitochondrial function in bEnd.3 cells through miR-155/SOCS6/p65 axis. (A–R) A series of loss- and gain-of-function experiments *in vitro* was conducted to verify the functional effects of exosomal miR-155/SOCS6/p65 axis on ROS generation and mitochondrial function. Rescue experiments for miR-155 overexpression were carried out by ectopic expression of SOCS6, and rescue experiments for miR-155 depletion were performed by SOCS6 depletion. (A-B and J-K) ROS level of bEnd.3 cells were detected and quantified by flow cytometry. (C-D and L-M) Immunofluorescence detection and quantification of MitoSOX in bEnd.3 cells (Scale bar = 50 μm). (E and N) Quantification of mitochondrial potential by JC-1 aggregates/JC-1 monomers. (F-G and O–P) Representative images of mitochondrial morphology and quantification of mitochondrial length and percentage of cells with fragmented mitochondria (Scale bar = 5 μm). (H–I and Q-R) OCR was used to evaluate mitochondrial functions of bEnd.3 cells. *P < 0.05, **P < 0.01.

recovery, these newborn vessels are highly permeable with TJs disruption; previous studies attributed this phenotype to chronic hypoxia [34]. As most human spinal cord injuries involve contusions of the spinal cord, most investigators have long used weight-drop contusion animal models to study the pathophysiology and genetic responses of spinal cord injury [28,29,35–39]. Notably, a comparative study between contusive SCI model and human SCI demonstrated an analogous relationship in rodent and human with respect to functional, electrophysiological, and morphological outcomes after SCI [40]. This indicated that contusive SCI model can serve as an adequate animal model for research on functional and morphological changes after SCI. Therefore, we used a mouse model of SCI contusive injury in this study to investigate the effects of infiltrated macrophages on vascular changes after SCI.

A previous study revealed that BSCB breakdown is an early event and precedes infiltration of peripheral immune cells such as neutrophils and macrophages [41]. It has been reported that macrophages are actively recruited to injured lesions and are predominantly located within the gray matter and dorsal funiculus white matter after SCI, presenting at 24 h, and peaking at 7 days post-injury [42,43]. Notably, although both M1 and M2 macrophages are present in the injured spinal cord, the spinal cord environment favors polarization of predominantly M1 cytotoxic macrophages, especially in the early stage [44]. A time course of M1 and M2 markers expression further demonstrated that iNOS was maximally increased 1–3 dpi, whose fold change was more significant than M2 markers in the early stage after SCI [13]. Macrophages and microglia appear to be double-edged swords for blood vessels. For instance, Faraco et al. proposed that perivascular macrophages play a pathogenic role in neurovascular dysfunction by generating large amounts of ROS [45], and increased infiltrated macrophages could significantly alter BBB-related gene expression in patients with schizophrenia by mediating neuroinflammation [46]. In addition, by suppressing proinflammatory responses of microglia and macrophages, Angiopoietin-2 blockade could improve BBB integrity in autoimmune encephalomyelitis [47]. Notably, macrophages also exert a positive effect on angiogenesis in traumatic brain injury by clearing fibrin and producing matrix metalloproteinase MMP-2[48]. Furthermore, as resident immune cells in CNS, microglia play a dual role in BBB integrity in systemic inflammation; during the early stages, microglia maintain BBB permeability via expression of TJs protein, while during sustained inflammation, microglia phagocytoses astrocyte end-feet and impairs BBB function [49]. These phenomena might be explained by broad M1 and M2 classification; however, there has been limited research directly and systematically investigating the effects of M1-macrophages on blood vessels after SCI. Based on our results, we found macrophage-vessel accumulation in injured area after SCI, and M1 polarization accounted for a substantial part of macrophage phenotype, which were consistent with previous studies [13,44]. We then validated that M1-BMDMs not only promoted EndoMT of vascular endothelial cells *in vitro* and *in vivo*, but also resulted in mitochondrial dysfunction by increasing mitochondrial ROS level, and the exosomal miR-155/SOCS6/p65 axis was involved in this process.

As a specific form of epithelial-to-mesenchymal transition (EMT), EndoMT process is characterized by the loss of apico-basal polarity and cell-cell adhesions in addition to the enhancement of front-back polarity and cell-matrix interactions [50]. EndoMT plays a critical role in vascular pathology by degrading TJs proteins and attenuating vascular markers while enhancing fibroblast markers expression [51–53]. In CNS diseases, Zhou et al. reported that myelin debris engulfment induced EndoMT of microvascular endothelial cells by reducing CD31 expression and upregulating α-SMA level after SCI [54]. Moreover, EndoMT is considered to be involved in LPS-induced damage to BBB integrity, and Bai et al. demonstrated EndoMT in strokes regulates BBB integrity by attenuating TJs protein levels and upregulating collagen I, III and α-SMA expression [55]. Collectively, EndoMT plays an important role in vascular pathology, and suppressing EndoMT after SCI may effectively preserve the newborn vascular and ameliorate BSCB integrity.

In vascular endothelial cells, mitochondrial ROS are byproducts during oxygen consumption, and high level of ROS can impair vascular function by regulating inflammation, proliferation, and mitophagy, which determines its wrecking role in BSCB integrity. It was reported that ROS were associated with silica nanoparticles-induced TJs loss and BBB disruption [56], and targeting scavenging ROS in vascular endothelial cells could eliminate the oxidative stress induced by ischemia-hypoxia, thus BBB integrity could be protected [31]. Moreover, Chen et al. demonstrated suppressing Sirt1 significantly attenuated mitochondrial ROS generation in strokes, which subsequently contributed to BBB integrity protection.

In our study, we validated that M1-BMDMs-induced EndoMT and mitochondrial ROS were mediated by exosomal transfer of miR-155 followed by suppression of SOCS6-induced p65 degradation. Through paracrine effect, exosomes could construct cell-to-cell communication by delivering genetic materials, and their role as a therapy or a "messenger" in SCI has been widely investigated in recent years [18,30]. It is well established that miR-155 is upregulated in M1-polarized macrophages to induce inflammation. For instance, miR-155 KO could alter Kupffer cells polarization from M1 to M2 and protect against alcohol-induced steatosis and inflammation [57]. In addition, exosomal miR-155 derived from macrophages was reported to be transferred into cardiac fibroblasts to induce cardiac inflammation [58], and suppressing miR-155 could alleviate proinflammation effect of macrophages in ulcerative colitis [59]. Also, it was reported that miR-155 is up-regulated after CNS injury with a time dependence, especially in $CD11b^{+}$ macrophages and microglia, and NOX deficiency could alter its expression and reduce ROS production [60]. Another study showed miR-155 deletion could significantly attenuate inflammation signaling in macrophages and reduce macrophages-induced neuron toxicity [61]. Taken these reported studies and our research together, downregulating miR-155 or preventing its transfer might contribute to SCI recovery.

SOCS6 belongs to the family of SOCS proteins, several of which have been characterized as negative-feedback regulators for cytokine receptor signaling [62]. SOCS6 was reported as a component of ubiquitin ligase, which inhibits assembly and disassembly of focal adhesions in migrating epithelial cells [63]. All SOCS family proteins share the same principal structure with a central SH2 domain and a SOCS box. A previous study revealed that SH2 domain is required for SOCS1 binding to p65, and that SOCS box accounts for the subsequent ubiquitination and proteasomal degradation of p65[64]. Moreover, SOCS3 was reported to inhibit expression and activity of p65 by interacting with it and induce its ubiquitin-dependent proteasomal degradation, and SH2 domain plays a crucial role in p65 binding and degradation. Given that SOCS6, SOCS1, and SOCS3 all belong to SOCS family, we assume that the SOCS6-induced p65 proteasomal degradation in our work might be in this manner as well. Notably, the protein levels of SOCS1 and SOCS3 following miR-155 overexpression or knockdown remain unchanged, which means that miR-155-regulated NF-κB pathway is independent on SOCS1 or SOCS3. As a post-translational modification, ubiquitination regulates the degradation of target proteins by attaching ubiquitin molecules to substrates. As a crucial transcription regulator, p65 nuclear translocation, which is an indicator of NF-κB signaling pathway activation, could affect downstream genes expression and then regulate neuroinflammation in SCI. Notably, the NF-κB signaling pathway was reported to participated in the vascular barrier dysfunction [65]. Moreover, in gastrointestinal inflammation, NF-κB activation in endothelial cells was reported along with mitochondrial ROS generation and TJs loss [66]. Similar results were observed in Alzheimer's disease, where beta amyloid-exposed bEnd.3 cells presented higher ROS levels and less TJs via NF-κB-mediated neuroinflammation. All these studies demonstrated that the NF-κB pathway was closely related with ROS generation and TJs breakdown, which accounted for the vascular barrier disruption.

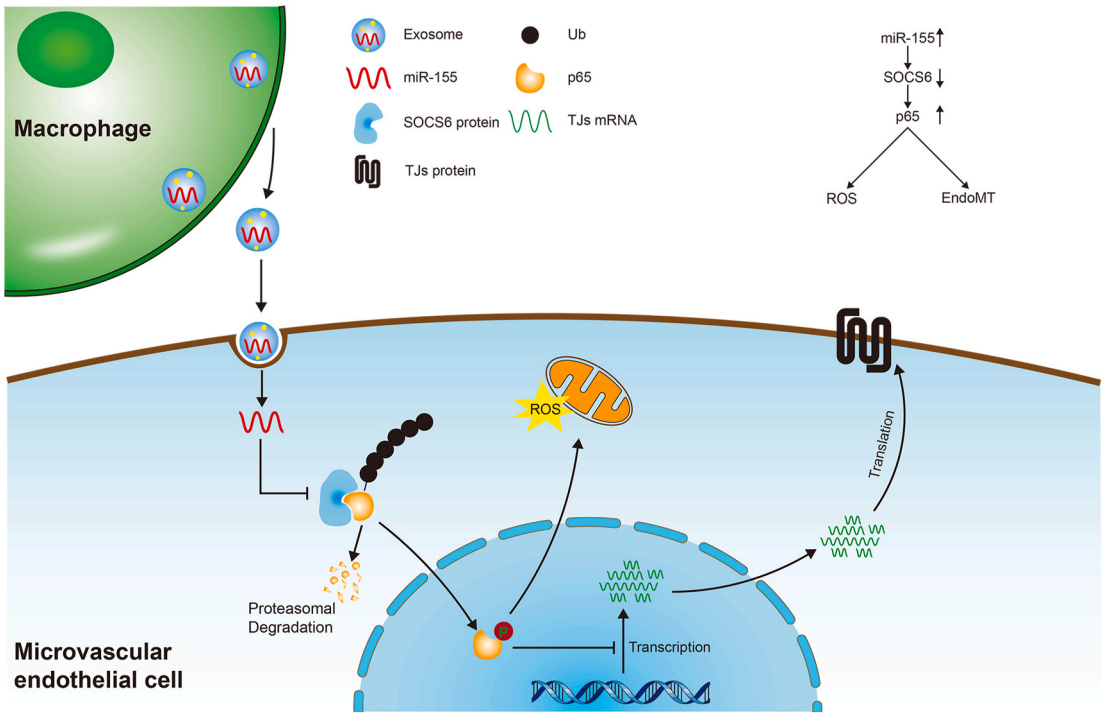

Fig. 11. Exosomal miR-155 from M1-polarized macrophages promotes EndoMT and impairs mitochondrial function in vascular endothelial cells after SCI. MiR-155 is transferred from M1-polarized macrophages to microvascular endothelial cells through exosomes, and internalized miR-155 targets and decreases SOCS6 which can ubiquitylate and degrade p65 in cytoplasm. The p65 proteasomal degradation is then suppressed and p65 nuclear translocation is upregulated, which subsequently promotes EndoMT and ROS generation in vascular endothelial cells.

5. Conclusion

In the present study, we demonstrated that infiltrated macrophages after SCI could aggravate BSCB integrity by promoting EndoMT and impairing mitochondrial function in vascular endothelial cells by delivering exosomal miR-155, and subsequently activating the NF-κB pathway by suppressing SOCS6-induced p65 degradation (Fig. 11). Our work might strengthen the comprehension of crosstalk between macrophages and vascular endothelial cells and uncover a potential mechanism in the regulation of BSCB integrity after SCI.

Declaration of competing interest

The authors declare that they have no known competing financial interests or personal relationships that could have appeared to influence the work reported in this paper.

Acknowledgements

This work was sponsored by the National Natural Science Foundation of China (Grant No.81974335); Natural Science Foundation of Jiangsu Province (Grant No. BK20181490); Postgraduate Research & Practice Innovation Program of Jiangsu Province (Grant No. SJCX20_0475); Six Talent Peaks Project in Jiangsu Province (Grant No. TD-SWYY-010), and Wu Jieping Medical Foundation (Grant No.320-2745-16-117).

Appendix A. Supplementary data

Supplementary data to this article can be found online at https://doi.org/10.1016/j.redox.2021.101932.

References

[1] J.T. Maikos, D.I. Shreiber, Immediate damage to the blood-spinal cord barrier due to mechanical trauma, J. Neurotrauma 24 (3) (2007) 492–507, https://doi.org/10.1089/neu.2006.0149.
[2] P.J. Horner, P.G. Popovich, B.B. Mullin, B.T. Stokes, A quantitative spatial analysis of the blood-spinal cord barrier. II. Permeability after intraspinal fetal transplantation, Exp. Neurol. 142 (2) (1996) 226–243, https://doi.org/10.1006/exnr.1996.0194.
[3] A.P. Tran, P.M. Warren, J. Silver, The biology of regeneration failure and success after spinal cord injury, Physiol. Rev. 98 (2) (2018) 881–917, https://doi.org/10.1152/physrev.00017.2017.
[4] E.A. Winkler, R.D. Bell, B.V. Zlokovic, Central nervous system pericytes in health and disease, Nat. Neurosci. 14 (11) (2011) 1398–1405, https://doi.org/10.1038/nn.2946.
[5] D. Yeung, J.L. Manias, D.J. Stewart, S. Nag, Decreased junctional adhesion molecule-A expression during blood-brain barrier breakdown, Acta Neuropathol. 115 (6) (2008) 635–642, https://doi.org/10.1007/s00401-008-0364-4.
[6] J.Y. Lee, H.S. Kim, H.Y. Choi, T.H. Oh, T.Y. Yune, Fluoxetine inhibits matrix metalloprotease activation and prevents disruption of blood-spinal cord barrier after spinal cord injury, Brain 135 (Pt 8) (2012) 2375–2389, https://doi.org/10.1093/brain/aws171.
[7] S. Nag, R. Venugopalan, D.J. Stewart, Increased caveolin-1 expression precedes decreased expression of occludin and claudin-5 during blood-brain barrier breakdown, Acta Neuropathol. 114 (5) (2007) 459–469, https://doi.org/10.1007/s00401-007-0274-x.
[8] J. Chen, G. Chen, J. Li, C. Qian, H. Mo, C. Gu, et al., Melatonin attenuates inflammatory response-induced brain edema in early brain injury following a subarachnoid hemorrhage: a possible role for the regulation of pro-inflammatory cytokines, J. Pineal Res. 57 (3) (2014) 340–347, https://doi.org/10.1111/jpi.12173.
[9] J. Bischoff, Endothelial-to-Mesenchymal transition purposeful versus maladaptive differentiation, Circ. Res. 124 (8) (2019) 1163–1165, https://doi.org/10.1161/Circresaha.119.314813.
[10] A.K. Shenoy, Y. Jin, H. Luo, M. Tang, C. Pampo, R. Shao, et al., Epithelial-to-mesenchymal transition confers pericyte properties on cancer cells, J. Clin. Invest. 126 (11) (2016) 4174–4186, https://doi.org/10.1172/JCI86623.
[11] X. Jiang, A.V. Andjelkovic, L. Zhu, T. Yang, M.V.L. Bennett, J. Chen, et al., Blood-brain barrier dysfunction and recovery after ischemic stroke, Prog. Neurobiol. 163 (2018), https://doi.org/10.1016/j.pneurobio.2017.10.001, 164144-171.
[12] K. Kobayakawa, Y. Ohkawa, S. Yoshizaki, T. Tamaru, T. Saito, K. Kijima, et al., Macrophage centripetal migration drives spontaneous healing process after spinal cord injury, Sci. Adv. 5 (5) (2019), eaav5086, https://doi.org/10.1126/sciadv.aav5086.

[13] K.A. Kigerl, J.C. Gensel, D.P. Ankeny, J.K. Alexander, D.J. Donnelly, P.G. Popovich, Identification of two distinct macrophage subsets with divergent effects causing either neurotoxicity or regeneration in the injured mouse spinal cord, J. Neurosci. 29 (43) (2009) 13435–13444, https://doi.org/10.1523/Jneurosci.3257-09.2009.
[14] L.M. Milich, C.B. Ryan, J.K. Lee, The origin, fate, and contribution of macrophages to spinal cord injury pathology, Acta Neuropathol. 137 (5) (2019) 785–797, https://doi.org/10.1007/s00401-019-01992-3.
[15] T. Okada, H. Suzuki, Z.D. Travis, J.H. Zhang, The stroke-induced blood-brain barrier disruption: current progress of inspection technique, mechanism, and therapeutic target, Curr. Neuropharmacol. (2020), https://doi.org/10.2174/1570159X18666200528143301.
[16] R. Kalluri, V.S. LeBleu, The biology, function, and biomedical applications of exosomes, Science 367 (6478) (2020), https://doi.org/10.1126/science.aau6977.
[17] M.A. Mori, R.G. Ludwig, R. Garcia-Martin, B.B. Brandao, C.R. Kahn, Extracellular miRNAs: from biomarkers to mediators of physiology and disease, Cell Metabol. 30 (4) (2019) 656–673, https://doi.org/10.1016/j.cmet.2019.07.011.
[18] W. Liu, Y. Wang, F. Gong, Y. Rong, Y. Luo, P. Tang, et al., Exosomes derived from bone mesenchymal stem cells repair traumatic spinal cord injury by suppressing the activation of A1 neurotoxic reactive astrocytes, J. Neurotrauma 36 (3) (2019) 469–484, https://doi.org/10.1089/neu.2018.5835.
[19] L. Li, Y. Zhang, J. Mu, J. Chen, C. Zhang, H. Cao, et al., Transplantation of human mesenchymal stem-cell-derived exosomes immobilized in an adhesive hydrogel for effective treatment of spinal cord injury 20 (6) (2020) 4298–4305, https://doi.org/10.1021/acs.nanolett.0c00929.
[20] A. Hervera, F. De Virgiliis, I. Palmisano, L.M. Zhou, E. Tantardini, G.P. Kong, et al., Reactive oxygen species regulate axonal regeneration through the release of exosomal NADPH oxidase 2 complexes into injured axons, Nat. Cell Biol. 20 (3) (2018) 307, https://doi.org/10.1038/s41556-018-0039-x.
[21] J. Wang, Y. Rong, C. Ji, C. Lv, D. Jiang, X. Ge, et al., MicroRNA-421-3p-abundant small extracellular vesicles derived from M2 bone marrow-derived macrophages attenuate apoptosis and promote motor function recovery via inhibition of mTOR in spinal cord injury, J. Nanobiotechnol. 18 (1) (2020) 72, https://doi.org/10.1186/s12951-020-00630-5.
[22] H. Sies, D.P. Jones, Reactive oxygen species (ROS) as pleiotropic physiological signalling agents, Nat. Rev. Mol. Cell Biol. 21 (7) (2020) 363–383, https://doi.org/10.1038/s41580-020-0230-3.
[23] N.P. Visavadiya, S.P. Patel, J.L. VanRooyen, P.G. Sullivan, A.G. Rabchevsky, Cellular and subcellular oxidative stress parameters following severe spinal cord injury, Redox Biol. (2016) 859–867, https://doi.org/10.1016/j.redox.2015.12.011.
[24] S.S. Andrabi, J. Yang, Y. Gao, Y.Z. Kuang, V. Labhasetwar, Nanoparticles with antioxidant enzymes protect injured spinal cord from neuronal cell apoptosis by attenuating mitochondrial dysfunction, J. Contr. Release (2020) 317300–317311, https://doi.org/10.1016/j.jconrel.2019.12.001.
[25] B.K. Lee, S.W. Hyun, Y.S. Jung, Yuzu and hesperidin ameliorate blood-brain barrier disruption during hypoxia via antioxidant activity, Antioxidants-Basel 9 (9) (2020). ARTN 84310.3390/antiox9090843.
[26] Y. Hong, H. Tak, C. Kim, H. Kang, E. Ji, S. Ahn, et al., RNA binding protein HuD contributes to beta-cell dysfunction by impairing mitochondria dynamics, Cell Death Differ. 27 (5) (2020) 1633–1643, https://doi.org/10.1038/s41418-019-0447-x.
[27] M. Khacho, A. Clark, D.S. Svoboda, J. Azzi, J.G. MacLaurin, C. Meghaizel, et al., Mitochondrial dynamics impacts stem cell identity and fate decisions by regulating a nuclear transcriptional Program, Cell Stem Cell 19 (2) (2016) 232–247, https://doi.org/10.1016/j.stem.2016.04.015.
[28] W. Liu, Y. Rong, J. Wang, Z. Zhou, X. Ge, C. Ji, et al., Exosome-shuttled miR-216a-5p from hypoxic preconditioned mesenchymal stem cells repair traumatic spinal cord injury by shifting microglial M1/M2 polarization, J. Neuroinflammation 17 (1) (2020) 47, https://doi.org/10.1186/s12974-020-1726-7.
[29] X. Zhou, S. Wahane, M.S. Friedl, M. Kluge, C.C. Friedel, K. Avrampou, et al., Microglia and macrophages promote corralling, wound compaction and recovery after spinal cord injury via Plexin-B2, Nat. Neurosci. 23 (3) (2020) 337–350, https://doi.org/10.1038/s41593-020-0597-7.
[30] D. Jiang, F. Gong, X. Ge, C. Lv, C. Huang, S. Feng, et al., Neuron-derived exosomes-transmitted miR-124-3p protect traumatically injured spinal cord by suppressing the activation of neurotoxic microglia and astrocytes, J. Nanobiotechnol. 18 (1) (2020) 105, https://doi.org/10.1186/s12951-020-00665-8.
[31] Q.Q. Bao, P. Hu, Y.Y. Xu, T.S. Cheng, C.Y. Wei, L.M. Pan, et al., Simultaneous blood-brain barrier crossing and protection for stroke treatment based on edaravone-loaded ceria nanoparticles, ACS Nano 12 (7) (2018) 6794–6805, https://doi.org/10.1021/acsnano.8b01994.
[32] V. Bartanusz, D. Jezova, B. Alajajian, M. Digicaylioglu, The blood-spinal cord barrier: morphology and clinical implications, Ann. Neurol. 70 (2) (2011) 194–206, https://doi.org/10.1002/ana.22421.
[33] J. Ruschel, F. Hellal, K.C. Flynn, S. Dupraz, D.A. Elliott, A. Tedeschi, et al., Axonal regeneration. Systemic administration of epothilone B promotes axon regeneration after spinal cord injury, Science 348 (6232) (2015) 347–352, https://doi.org/10.1126/science.aaa2958.
[34] Y. Yang, S. Kimura-Ohba, J.F. Thompson, V.M. Salayandia, M. Cosse, L. Raz, et al., Vascular tight junction disruption and angiogenesis in spontaneously hypertensive rat with neuroinflammatory white matter injury, Neurobiol. Dis. (2018), https://doi.org/10.1016/j.nbd.2018.02.012, 11495-110.
[35] A.Z. Akhtar, J.J. Pippin, C.B. Sandusky, Animal models in spinal cord injury: a review, Rev. Neurosci. 19 (1) (2008) 47–60, https://doi.org/10.1515/revneuro.2008.19.1.47.
[36] V. Bellver-Landete, F. Bretheau, B. Mailhot, N. Vallieres, M. Lessard, M.E. Janelle, et al., Microglia are an essential component of the neuroprotective scar that forms after spinal cord injury, Nat. Commun. 10 (2019), 518, https://doi.org/10.1038/s41467-019-08446-0.
[37] K. Kobayakawa, Y. Ohkawa, S. Yoshizaki, T. Tamaru, T. Saito, K. Kijima, et al., Macrophage centripetal migration drives spontaneous healing process after spinal cord injury, Sci. Adv. 5 (5) (2019), eaav5086, https://doi.org/10.1126/sciadv.aav5086.
[38] A.L. Vivinetto, I.D. Kim, D.C. Goldberg, L. Fones, E. Brown, V.S. Tarabykin, et al., Zeb2 is a regulator of astrogliosis and functional recovery after CNS injury, Cell Rep. 31 (13) (2020), 107834, https://doi.org/10.1016/j.celrep.2020.107834.
[39] W. Young, Spinal cord contusion models, Prog. Brain Res. (2002) 137231–137255, https://doi.org/10.1016/s0079-6123(02)37019-5.
[40] G.A. Metz, A. Curt, H. van de Meent, I. Klusman, M.E. Schwab, V. Dietz, Validation of the weight-drop contusion model in rats: a comparative study of human spinal cord injury, J. Neurotrauma 17 (1) (2000) 1–17, https://doi.org/10.1089/neu.2000.17.1.
[41] S. Floris, E.L. Blezer, G. Schreibelt, E. Dopp, S.M. van der Pol, I.L. Schadee-Eestermans, et al., Blood-brain barrier permeability and monocyte infiltration in experimental allergic encephalomyelitis: a quantitative MRI study, Brain 127 (Pt 3) (2004) 616–627, https://doi.org/10.1093/brain/awh068.
[42] S.L. Carlson, M.E. Parrish, J.E. Springer, K. Doty, L. Dossett, Acute inflammatory response in spinal cord following impact injury, Exp. Neurol. 151 (1) (1998) 77–88, https://doi.org/10.1006/exnr.1998.6785.
[43] K.D. Beck, H.X. Nguyen, M.D. Galvan, D.L. Salazar, T.M. Woodruff, A.J. Anderson, Quantitative analysis of cellular inflammation after traumatic spinal cord injury: evidence for a multiphasic inflammatory response in the acute to chronic environment, Brain 133 (Pt 2) (2010) 433–447, https://doi.org/10.1093/brain/awp322.
[44] A. Kroner, A.D. Greenhalgh, J.G. Zarruk, R.P. dos Santos, M. Gaestel, S. David, TNF and increased intracellular iron alter macrophage polarization to a detrimental M1 phenotype in the injured spinal cord (vol 83, pg 1098, 2014), Neuron 86 (5) (2015), https://doi.org/10.1016/j.neuron.2015.05.029, 1317-1317.
[45] G. Faraco, Y. Sugiyama, D. Lane, L. Garcia-Bonilla, H. Chang, M.M. Santisteban, et al., Perivascular macrophages mediate the neurovascular and cognitive dysfunction associated with hypertension, J. Clin. Invest. 126 (12) (2016) 4674–4689, https://doi.org/10.1172/JCI86950.
[46] H.Q. Cai, V.S. Catts, M.J. Webster, C. Galletly, D. Liu, M. O'Donnell, et al., Increased macrophages and changed brain endothelial cell gene expression in the frontal cortex of people with schizophrenia displaying inflammation, Mol. Psychiatr. 25 (4) (2020) 761–775, https://doi.org/10.1038/s41380-018-0235-x.
[47] Z.L. Li, E.A. Korhonen, A. Merlini, J. Strauss, E. Wihuri, H. Nurmi, et al., Angiopoietin-2 blockade ameliorates autoimmune neuroinflammation by inhibiting leukocyte recruitment into the CNS, J. Clin. Invest. 130 (4) (2020) 1977–1990, https://doi.org/10.1172/Jci130308.
[48] M.V. Russo, L.L. Latour, D.B. McGavern, Distinct myeloid cell subsets promote meningeal remodeling and vascular repair after mild traumatic brain injury, Nat. Immunol. 19 (5) (2018) 442–452, https://doi.org/10.1038/s41590-018-0086-2.
[49] K. Haruwaka, A. Ikegami, Y. Tachibana, N. Ohno, H. Konishi, A. Hashimoto, et al., Dual microglia effects on blood brain barrier permeability induced by systemic inflammation, Nat. Commun. 10 (1) (2019) 5816, https://doi.org/10.1038/s41467-019-13812-z.
[50] J. Xiong, H. Kawagishi, Y. Yan, J. Liu, Q.S. Wells, L.R. Edmunds, et al., A metabolic basis for endothelial-to-mesenchymal transition, Mol. Cell 69 (4) (2018) 689–698, https://doi.org/10.1016/j.molcel.2018.01.010, e687.
[51] M. Manetti, E. Romano, I. Rosa, S. Guiducci, S. Bellando-Randone, A. De Paulis, et al., Endothelial-to-mesenchymal transition contributes to endothelial dysfunction and dermal fibrosis in systemic sclerosis, Ann. Rheum. Dis. 76 (5) (2017) 924–934, https://doi.org/10.1136/annrheumdis-2016-210229.
[52] M. Huang, T. Liu, P. Ma, R.A. Mitteer Jr., Z. Zhang, H.J. Kim, et al., c-Met-mediated endothelial plasticity drives aberrant vascularization and chemoresistance in glioblastoma, J. Clin. Invest. 126 (5) (2016) 1801–1814, https://doi.org/10.1172/JCI84876.
[53] P.Y. Chen, L. Qin, C. Barnes, K. Charisse, T. Yi, X. Zhang, et al., FGF regulates TGF-beta signaling and endothelial-to-mesenchymal transition via control of let-7 miRNA expression, Cell Rep. 2 (6) (2012) 1684–1696, https://doi.org/10.1016/j.celrep.2012.10.021.
[54] T. Zhou, Y. Zheng, L. Sun, S.R. Badea, Y. Jin, Y. Liu, et al., Microvascular endothelial cells engulf myelin debris and promote macrophage recruitment and fibrosis after neural injury, Nat. Neurosci. 22 (3) (2019) 421–435, https://doi.org/10.1038/s41593-018-0324-9.
[55] Y. Bai, Y. Zhang, B. Han, L. Yang, X. Chen, R. Huang, et al., Circular RNA DLGAP4 ameliorates ischemic stroke outcomes by targeting miR-143 to regulate endothelial-mesenchymal transition associated with blood-brain barrier integrity, J. Neurosci. 38 (1) (2018) 32–50, https://doi.org/10.1523/JNEUROSCI.1348-17.2017.
[56] X. Liu, B.Y. Sui, J. Sun, Blood-brain barrier dysfunction induced by silica NPs in vitro and in vivo: involvement of oxidative stress and Rho-kinase/JNK signaling pathways, Biomaterials (2017) 12164–12182, https://doi.org/10.1016/j.biomaterials.2017.01.006.
[57] S. Bala, T. Csak, B. Saha, J. Zatsiorsky, K. Kodys, D. Catalano, et al., The pro-inflammatory effects of miR-155 promote liver fibrosis and alcohol-induced steatohepatitis, J. Hepatol. 64 (6) (2016) 1378–1387, https://doi.org/10.1016/j.jhep.2016.01.035.
[58] C. Wang, C. Zhang, L. Liu, A X, B. Chen, Y. Li, et al., Macrophage-derived mir-155-containing exosomes suppress fibroblast proliferation and promote fibroblast

inflammation during cardiac injury, Mol. Ther. 25 (1) (2017) 192–204, https://doi.org/10.1016/j.ymthe.2016.09.001.
[59] S. Qu, Y. Shen, M. Wang, X. Wang, Y. Yang, Suppression of miR-21 and miR-155 of macrophage by cinnamaldehyde ameliorates ulcerative colitis, Int. Immunopharm. (2019) 6722–6734, https://doi.org/10.1016/j.intimp.2018.11.045.
[60] B. Sabirzhanov, Y. Li, M. Coll-Miro, J.J. Matyas, J. He, A. Kumar, et al., Inhibition of NOX2 signaling limits pain-related behavior and improves motor function in male mice after spinal cord injury: participation of IL-10/miR-155 pathways, Brain Behav. Immun. (2019) 8073–8087, https://doi.org/10.1016/j.bbi.2019.02.024.
[61] A.D. Gaudet, S. Mandrekar-Colucci, J.C. Hall, D.R. Sweet, P.J. Schmitt, X. Xu, et al., miR-155 deletion in mice overcomes neuron-intrinsic and neuron-extrinsic barriers to spinal cord repair, J. Neurosci. 36 (32) (2016) 8516–8532, https://doi.org/10.1523/JNEUROSCI.0735-16.2016.
[62] B. Wang, E. Wangkahart, C.J. Secombes, T.H. Wang, Insights into the evolution of the suppressors of cytokine signaling (SOCS) gene family in vertebrates, Mol. Biol. Evol. 36 (2) (2019) 393–411, https://doi.org/10.1093/molbev/msy230.
[63] A. Teckchandani, J.A. Cooper, The ubiquitin-proteasome system regulates focal adhesions at the leading edge of migrating cells, eLife 5 (2016), e17440, https://doi.org/10.7554/eLife.17440.
[64] J. Strebovsky, P. Walker, R. Lang, A.H. Dalpke, Suppressor of cytokine signaling 1 (SOCS1) limits NF kappa B signaling by decreasing p65 stability within the cell nucleus, Faseb. J. 25 (3) (2011) 863–874, https://doi.org/10.1096/fj.10-170597.
[65] B. Kim, C. Jang, H. Dharaneeswaran, J. Li, M. Bhide, S. Yang, et al., Endothelial pyruvate kinase M2 maintains vascular integrity, J. Clin. Invest. 128 (10) (2018) 4543–4556, https://doi.org/10.1172/Jci120912.
[66] E.A. Mutlu, P.A. Engen, S. Soberanes, D. Urich, C.B. Forsyth, R. Nigdelioglu, et al., Particulate matter air pollution causes oxidant-mediated increase in gut permeability in mice, Part. Fibre Toxicol. 8 (2011), 19, https://doi.org/10.1186/1743-8977-8-19.